Contrib Mineral Petrol (2006) 152:611–638
DOI 10.1007/s00410-006-0123-2

ORIGINAL PAPER

Effect of water on tholeiitic basalt phase equilibria: an experimental study under oxidizing conditions

Sandrin T. Feig · Jürgen Koepke · Jonathan E. Snow

Received: 18 November 2005 / Accepted: 14 June 2006 / Published online: 15 August 2006

Abstract To investigate the effect of water on phase relations and compositions in a basaltic system, we performed crystallization experiments at pressures of 100, 200 and 500 MPa in a temperature range of 940 to 1,220°C using four different water contents. Depending on the water activity, the oxygen fugacity varied between 1 and 4 log units above the quartz-magnetite-fayalite buffer. Addition of water to the dry system shifts the solidus > 250°C to lower temperatures and increases the amount of melt drastically. For instance, at 1,100°C and 200 MPa, the melt fraction increases from 12.5 wt% at a water content of 1.6 wt% to 96.3% at a water content of 5 wt% in the melt. The compositions of the experimental phases also show a strong effect of water. Plagioclase is shifted to higher anorthite contents by the addition of water. Olivine and clinopyroxene show generally higher MgO/FeO ratios with added water, which could also be related to the increasing oxygen fugacity with water. Moreover, water affects the partitioning of certain elements between minerals and melts, e.g., the Ca partitioning between olivine and melt. Plagioclase shows a characteristic change in the order of crystallization with water that may help to explain the formation of wehrlites intruding the lower oceanic crust (e.g., in Oman, Macquarie Island). At 100 MPa, plagioclase crystallizes before clinopyroxene at all water contents. At pressures > 100 MPa, plagioclase crystallizes before clinopyroxene at low water contents (e.g. < 3 wt%), but after clinopyroxene at H_2O in the melt > 3 wt%. This change in crystallization order indicates that a paragenesis typical for wehrlites (olivine–clinopyroxene–without plagioclase) is stabilized at low pressures typical of the oceanic crust only at high water contents. This opens the possibility that typical wehrlites in the oceanic crust can be formed by the fractionation and accumulation of olivine and clinopyroxene at 1,060°C and > 100 MPa in a primitive tholeiitic basaltic system containing more than 3 wt% water. The comparison of the experimental results with evolution trends calculated by the thermodynamic models ''MELTS'' and ''Comagmat'' shows that neither model predicts the experimental phase relations with sufficient accuracy.

Communicated by J. Hoefs

Electronic Supplementary Material Supplementary material is available for this article at http://dx.doi.org/10.1007/s00410-006-0123-2 and is accessible for authorized users.

S. T. Feig (✉) · J. Koepke
Institute of Mineralogy, University of Hannover,
Callinstr. 3, 30167 Hannover, Germany
e-mail: S.Feig@Mineralogie.Uni-Hannover.de

J. E. Snow
Max-Planck-Institute for Chemistry,
Postfach 3060, 55020 Mainz, Germany

Present Address:
J. E. Snow
Department of Geosciences, University of Houston,
Houston, TX 77204-5007, USA

Introduction

Water plays an important role in several aspects of seafloor magmatic processes. For a long time, it was considered that crystallization at mid-ocean ridges takes place under nearly ''dry'' conditions. During the last decade, improvements in analytical techniques

have made it possible to determine small amounts of water in quenched MORB glasses (e.g., Kovalenko et al. 2000), in glass inclusions (e.g., Danyushevsky et al. 2000; Saal et al. 2002; Sobolev and Chaussidon 1996) and even in nominally dry minerals of the upper mantle (e.g., Bell and Rossman 1992; Hirschmann et al. 2005). Small amounts of water (< 1 wt%) may have a significant effect on MORB petrogenesis (Danyushevsky 2001), from partial melting of the mantle to fractionation (Asimow and Langmuir 2003). Moreover, it is well known that water plays a significant role in late-stage magmatic processes during ocean crust formation, since water can be enriched during differentiation resulting in the formation of typical interstitial amphiboles (e.g., Coogan et al. 2001; Tribuzio et al. 2000). Finally, recent papers show that very high temperature (1,200°C) hydrothermal activity triggers hydrous melting processes (Boudier et al. 2005; Koepke et al. 2005c; Koepke et al. 2004; Nicolas et al. 2003). Therefore, it is important to quantify the role of water both on the phase equilibria and on the mineral and melt compositions in MORB-type systems.

In this study, we present new crystallization experiments on a tholeiitic basalt composition from the Southwest Indian Ridge (SWIR). We systematically varied the water content and the pressure from near-surface conditions to those expected in the upper mantle at a slow-spreading ridge (e.g. Shipboard Scientific Party 2004).

The experiments vary in oxygen fugacity (fO_2) between QFM + 1 and QFM + 4 (QFM: quartz-magnetite-fayalite buffer), which is in general more oxidized compared to typical mid-ocean ridge conditions. The oxygen fugacity of erupted primitive MORB melts vary between QFM + 1 to QFM − 2 (Bezos and Humler 2005; Christie et al. 1986). Thus, direct comparison between these results and cogenetic MORB suites is not straightforward. However, it is true that in drilled cumulate sections, the abundance of oxide gabbros (e.g. Natland and Dick 2002; Natland et al. 1991) suggests that more oxidizing conditions may characterize the middle crust than the mantle sources. This experimental investigation shows for the first time the systematic effect on the water and shallow pressure dependence of phase equilibria in a primitive tholeiitic basaltic system under fO_2 conditions, corresponding to the upper level of redox conditions known from nature. A second phase equilibria study in the same system under more reducing conditions QFM + 2 (QFM + 2 to − 1, depending on the water activity) and QFM (QFM + 0 to − 3, depending on the water activity) is in progress.

Previous experimental work

Most of the experiments in tholeiitic basaltic systems thus far were performed at 1 atm (e.g. Grove and Baker 1984; Grove and Bryan 1983; Juster et al. 1989; Sano et al. 2001; Thy et al. 1998, 1999), revealing the well-known crystallization sequence of MORB. Further experiments were performed in gas mixture furnaces at 1 atm to identify the effect of different redox conditions on the chemistry of the experimental products (e.g., Snyder et al. 1993; Toplis and Carroll 1995). These experiments show that mainly the stability and the composition of iron-bearing phases (e.g., olivine, clinopyroxene and magnetite) are affected by the oxygen fugacity.

On the other hand, experiments in water-bearing systems under shallow pressures are limited in number. The first water-bearing phase equilibria experiments on tholeiitic basalts under pressures below 500 MPa showed that the formation of quench-crystals during cooling was almost unavoidable (e.g. Eggler and Burnham 1973; Hamilton et al. 1964; Helz 1973, 1976; Holloway and Burnham 1972). Such experiments do not allow adequate analyses of the glass phase, and it is very difficult to distinguish between quench and equilibrium crystallization. To reach higher quenching rates, a rapid quench system was developed for internally heated pressure vessels (Berndt et al. 2002; Holloway et al. 1992; Roux and Lefevre 1992), which allowed the experimental melts to be quenched to homogeneous glasses.

Most experiments on water-bearing tholeiitic basalts are typically carried out under water-saturated conditions. Sisson and Grove (1993a, b) conducted experiments in a calc-alkaline system under water-saturated conditions at 200 MPa. Spulber and Rutherford (1983) performed experiments in a MORB system from the Galapagos Spreading Center. There are also experiments at reduced water activities like Holloway and Burnham (1972) who studied a tholeiitic basalt from the Kilauea volcano and Kawamoto (1996) who performed experiments in a calc-alkaline system at a water activity < 1. All these authors observed a strong effect of water on phase relations in the system. Aside from general effects like the stability of water-bearing phases (e.g. amphibole), effects on element partitioning were observed as well (Sisson and Grove 1993a, b). Gaetani et al. (1993, 1994) investigated experimentally a basaltic andesite system under dry and water-saturated conditions (200 MPa). They found that the crystallization order in a dry system is olivine–plagioclase–clinopyroxene, while it is changed in a water-saturated system to olivine–clinopyroxene–plagioclase.

Due to the fixed water content in most of the studies mentioned above, systematic effects of water on the phase equilibria and phase compositions could not be determined. The only experimental study where the water content was varied systematically under crustal pressure was conducted by Berndt et al. (2005). In their study, they added different amounts of water to a synthetic glass corresponding to a primitive MORB and constructed phase diagrams for the system at 200 MPa. With decreasing temperature the water content in the melt increases dramatically, due to ongoing crystallization. At low temperatures all experiments were water saturated. They observed a strong effect of the water activity and the water content of the system on the phase relations, phase chemistry and on the element partitioning. Furthermore, they showed that water has the ability to control differentiation trends.

Experimental techniques

As capsule material, gold (at temperatures < 1,060°C) and $Au_{80}Pd_{20}$ (at higher temperatures) were used. XH_2O [molar $H_2O/(H_2O + CO_2)$] of the fluid phase was varied. In each experimental run, four different XH_2O were applied: 0.0 (nominally dry), 0.2, 0.6 and 1.0 (water saturated). All experiments except the nominally dry were fluid saturated. XH_2O of 0.2 and 0.6 are fixed via mixtures of water and silver oxalate ($Ag_2C_2O_4$). We assume that CO_2 does not play an important role as chemical component in this system. For each run 10 to 40 mg of starting glass powder (pre-dried), and the desired amounts of water (using a micro syringe) and silver oxalate were transferred into the capsule. For the ''nominally dry'' runs, only glass powder was inserted into the capsule. These filled capsules were dried at 500°C for 10 min.

All experiments were performed in a vertically mounted internally heated pressure vessel (IHPV), equipped with a rapid quench system to prevent the formation of quench-crystals (Berndt et al. 2002; Holloway et al. 1992; Roux and Lefevre 1992), using pure argon as pressure medium. A detailed description of the apparatus is given by Berndt et al. (2002). All experiments were performed at an oxygen fugacity corresponding to the MnO–Mn_3O_4 buffer. Depending on a H_2O, the fO_2 of the experiments varies between ~ QFM + 1 and QFM + 4.2, which is in the upper level of the redox conditions known from nature (Bezos and Humler 2005; Christie et al. 1986). To apply this study to magma chamber processes of mid-ocean ridges, pressure conditions of 100, 200 and, taking into account the thick lithosphere at slow spreading ridges, 500 MPa were selected in the study. Additionally, the experiments at three different pressures also allow determining the effect of water as a function of pressure. To construct phase diagrams, experiments in the temperature range 940–1,220°C were performed. The temperature was measured with four S-type thermocouples, showing a gradient of less than 4°C along the sample and an uncertainty less than ± 10°C. The experimental conditions for each run are listed in Table 1.

After quenching, each capsule was weighed to check for leaks and then, punctured and immediately weighed again to check if CO_2 was present in the capsule. To check if water was present, the punctured capsule was dried at 130°C and weighed again.

Starting material

As a starting material for the experiments, we used a microgabbro from the SWIR. Microgabbros occur as small dikes with medium to fine-grained equigranular textures within the drilled gabbro section of the SWIR. According to Dick et al. (2000) these microgabbros represent melt transport channels through crystallizing intrusions. We used the microgabbro ''R6a'' (ODP designation: 176-735B-178R-6:132-138; Snow, 2002), recovered from a depth of 1219 mbsf (meters below sea floor) on ODP Leg 176. This rock exhibits a fine-grained (< 0.5 mm), equigranular texture consisting of plagioclase (55 mol% anorthite; ~ 65 vol% in the mode), olivine (71 mol% forsterite; ~ 15 vol% in the mode), clinopyroxene (Mg# = 79 (molar 100 × MgO/(MgO+FeO)); ~ 15 vol% in the mode) and interstitial phases (pargasitic amphibole, orthopyroxene, ilmenite, Cr-rich magnetite, and pyrite; ~ 5 vol% in the mode in total). The chemical composition of the gabbro is close to a primitive tholeiitic basalt (Table 2), but K_2O, TiO_2 and P_2O_5 are nonetheless somewhat low for such a composition. Therefore, we believe that this rock also includes a certain cumulate character.

The starting glass was prepared by crushing the sample and regrinding it in a rotary mortar. The rock was totally fused at 1,600°C in a platinum crucible and quenched with water. The homogeneity of the glass was confirmed by electron microprobe analyses. For the experimental runs, this glass was crushed to a grain size of < 150 μm and filled into noble metal capsules (10 to 40 mg for each run).

Table 1 Conditions and phases of the performed experiments

Run	Pressure (MPa)	Temperature (°C)	Duration (h)	H_2O in the melt (wt%)[a]	aH_2O[b]	logfO_2[c]	ΔQFM	Phases[d]						ΣR^2	K_D Ol-melt/ Fe-Mg[e]
#1	203.1	1,100 ± 4	30	5.0	1.00	− 5.21	+4.14	ol (2.8)	cr-sp (0.9)	glass (96.3)				0.13	0.33
#2	203.1	1,100 ± 4	30	2.9	0.49	− 5.83	+3.52	ol (9.9)	plag (24.6)	cpx (13.8)	glass (51.8)			0.35	0.34
#3	203.1	1,100 ± 4	30	1.9	0.30	− 6.26	+3.09	ol (12.0)	plag (43.3)	cpx (21.2)	mag (0.7)	glass (22.8)		0.02	0.35
#5	203.1	1,100 ± 4	30	1.6	0.23	− 6.49	+2.86	ol (12.3)	plag (51.4)	cpx (22.9)	mag (0.9)	glass (12.5)		0.02	0.36
#6	200.5	1,180 ± 2	30	4.9	1.00	− 4.19	+4.17	glass (100.0)							
#7	200.5	1,180 ± 2	30	3.0	0.54	− 4.72	+3.64	cr-sp	glass					–[f]	
#8	200.5	1,180 ± 2	30	2.1	0.31	− 5.20	+3.16	ol (1.7)	cr-sp (0.4)	glass (98.0)				0.45	0.46
#9	200.5	1,180 ± 2	30	0.8	0.06	− 6.65	+1.71	ol (3.1)	cr-sp (1.6)	glass (95.4)				1.89	0.38
#10	202.7	1,060 ± 3	30	5.1	1.00	− 5.77	+4.13	ol (6.2)	cpx (1.9)	cr-sp (0.7)	glass (91.2)			0.01	0.34
#11	202.7	1,060 ± 3	30	2.8	0.48	− 6.41	+3.49	ol (11.4)	plag (31.9)	cpx (18.3)	mag (0.6)	glass (37.9)		0.00	0.37
#12	202.7	1,060 ± 3	30	n.a.	–	–	–	ol	plag	cpx	opx	mag	glass	–[f]	
#13	202.7	1,060 ± 3	30	n.a.	–	–	–	ol	plag	cpx	opx	mag	glass	–[f]	
#14	201.9	1,140 ± 3	30	4.9	1.00	− 4.68	+4.16	cr-sp (1.3)	glass (98.7)					0.36	
#15	201.9	1,140 ± 3	30	2.8	0.46	− 5.35	+3.49	ol (4.0)	cr-sp (0.8)	glass (95.2)				0.09	0.38
#16	201.9	1,140 ± 3	30	1.7	0.24	− 5.91	+2.93	ol (10.7)	plag (26.1)	cpx (8.8)	glass (54.4)			0.09	0.39
#17	201.9	1,140 ± 3	30	1.5	0.20	− 6.10	+2.75	ol (11.2)	plag (31.8)	cpx (13.5)	glass (43.4)			0.31	0.42
#18	203.0	1,220 ± 2	20	1.9	0.28	− 4.82	+3.08	cr-sp (0.6)	glass (99.4)					0.10	
#19	203.0	1,220 ± 2	20	1.2	0.13	− 5.47	+2.43	cr-sp (0.7)	glass (99.3)					0.22	
#20	203.0	1,220 ± 2	20	0.6	0.04	− 6.57	+1.33	ol (1.4)	cr-sp (1.0)	glass (97.6)				0.94	0.33
#21	201.8	1,160 ± 2	24	4.9	1.00	− 4.44	+4.16	cr-sp (0.6)	glass (99.4)					0.30	
#22	201.8	1,160 ± 2	24	3.1	0.55	− 4.95	+3.64	ol (2.9)	cr-sp (1.2)	glass (95.9)				0.34	0.47
#23	201.8	1,160 ± 2	24	1.5	0.18	− 5.94	+2.66	ol (5.1)	plag (0.7)	cr-sp (0.9)	glass (93.3)			0.37	0.41
#24	201.8	1,160 ± 2	24	0.9	0.08	− 6.64	+1.96	ol (9.4)	plag (16.9)	cpx (4.4)	glass (69.3)			1.38	0.37
#25	203.5	1,020 ± 2	42	5.1	1.00	− 6.36	+4.11	ol (9.7)	plag (14.0)	cpx (14.6)	mag (1.2)	glass (60.5)		0.08	0.37
#26	203.5	1,020 ± 2	42	n.a.	–	–	–	ol	plag	cpx	mag	glass		–[f]	
#31	203.0	980 ± 1	43	5.2	1.00	− 6.99	+4.10	ol (0.9)	plag (18.0)	cpx (10.1)	amph (36.7)	mag (1.3)	glass (33.1)	0.00	0.34
#32	203.0	940 ± 4	68	5.3	1.00	− 7.66	+4.08	plag (20.2)	cpx (0.8)	opx (1.9)	amph (57.5)	mag (0.7)	glass (18.9)	0.01	
#38	104.7	1,180 ± 2	22	3.4	1.00	− 4.24	+4.18	cr-sp (0.7)	glass (99.3)					0.17	
#39	104.7	1,180 ± 2	22	1.5	0.30	− 5.30	+3.12	ol (2.4)	cr-sp (1.4)	glass (96.1)				0.77	0.45
#40	104.7	1,180 ± 2	22	1.2	0.20	− 5.65	+2.77	ol (3.5)	cr-sp (0.9)	glass (95.6)				0.74	0.45
#41	104.7	1,180 ± 2	22	0.7	0.08	− 6.46	+1.96	ol	plag	cr-sp	glass			–[g]	0.40
#42	102.2	1,100 ± 4	41	3.5	1.00	− 5.26	+4.16	ol (5.3)	cr-sp (1.0)	glass (93.8)				0.10	0.43
#44	102.2	1,100 ± 4	41	1.7	0.41	− 6.03	+3.39	ol (14.4)	plag (46.8)	cpx (18.7)	glass (20.1)			0.78	0.47
#45	102.2	1,100 ± 4	41	1.9	0.49	− 5.89	+3.53	ol (13.7)	plag (42.2)	cpx (16.7)	glass (27.4)			0.55	0.47
#46	101.5	1,160 ± 4	82	3.4	1.00	− 4.48	+4.18	cr-sp (0.9)	glass (99.1)					0.39	
#47	101.5	1,160 ± 4	82	2.1	0.48	− 5.11	+3.55	ol (2.8)	cr-sp (1.3)	glass (95.9)				0.78	0.45
#48	101.5	1,160 ± 4	82	1.0	0.15	− 6.14	+2.53	ol (5.4)	plag (3.1)	cpx (0.2)	cr-sp (2.8)	glass (88.4)		0.65	0.40
#49	101.5	1,160 ± 4	82	0.8	0.10	− 6.45	+2.21	ol (7.2)	plag (10.9)	cpx (2.2)	cr-sp (2.6)	glass (77.2)		1.75	0.39
#50	103.8	1,060 ± 2	42	3.5	1.00	− 5.83	+4.14	ol (10.2)	plag (14.0)	cpx (9.8)	glass (66.0)			0.14	0.46
#51	103.8	1,060 ± 2	42	2.1	0.52	− 6.39	+3.58	ol (14.5)	plag (40.1)	cpx (17.6)	glass (27.8)			0.20	0.45
#52	103.8	1,060 ± 2	42	n.a.	–	–	–	ol	plag	cpx	glass			–[f]	
#53	103.8	1,060 ± 2	42	1.8	0.34	− 6.77	+3.20	ol (15.5)	plag (48.5)	cpx (21.0)	glass (15.1)			0.33	0.41
#54	104.0	1,140 ± 2	22	3.4	1.00	− 4.74	+4.17	ol (2.2)	cr-sp (0.9)	glass (96.9)				0.11	0.39

Table 1 continued

Run	Pressure (MPa)	Temperature (°C)	Duration (h)	H_2O in the melt (wt%)[a]	aH_2O[b]	logfO_2[c]	ΔQFM	Phases[d]						ΣR^2	K_D Ol-melt/ Fe-Mg[e]
#55	104.0	1,140 ± 2	22	2.0	0.44	– 5.45	+3.46	ol (5.4)	plag (0.3)	cr-sp (0.5)	glass (93.8)			0.27	0.42
#56	104.0	1,140 ± 2	22	1.1	0.20	– 6.14	+2.77	ol (12.0)	plag (30.3)	cpx (8.6)	glass (49.1)			0.25	0.38
#57	104.0	1,140 ± 2	22	1.3	0.27	– 5.89	+3.02	ol (12.1)	plag (31.7)	cpx (8.9)	glass (47.3)			0.60	0.41
#58	100.9	980 ± 3	70	n.a.	–	–	–	ol	plag	cpx	opx	amph	mag glass	–[f]	
#67	501.0	1,160 ± 1	39	4.4	0.44	– 4.98	+3.42	ol (1.1)	cr-sp (0.8)	glass (98.1)				0.11	0.35
#68	501.0	1,160 ± 1	39	3.8	0.37	– 5.13	+3.27	ol (1.0)	cr-sp (1.1)	glass (97.9)				0.10	0.35
#69	501.0	1,160 ± 1	39	1.3	0.07	– 6.56	+1.84	ol (10.4)	plag (35.6)	cpx (20.1)	glass (33.9)			0.38	0.34
#70	502.0	1,100 ± 6	68	9.1	1.00	– 5.05	+4.10	ol (0.8)	cr-sp (0.7)	glass (98.5)				0.15	0.36
#71	502.0	1,100 ± 6	68	3.6	0.31	– 6.05	+3.09	ol	plag	cpx	opx	glass		–[g]	0.40
#72	502.0	1,100 ± 6	68	2.8	0.22	– 6.35	+2.80	ol	plag	cpx	opx	glass		–[g]	0.38
#73	502.0	1,100 ± 6	68	n.a.	–	–	–	ol	plag	cpx	opx	mag	glass	–[f]	
#74	501.7	1,130 ± 4	42	9.2	1.00	– 4.65	+4.12	cr-sp (0.8)	glass (99.2)					0.41	
#75	501.7	1,130 ± 4	42	4.4	0.41	– 5.42	+3.34	ol (3.4)	cpx (3.3)	cr-sp (0.8)	glass (92.5)			0.04	0.34
#76	501.7	1,130 ± 4	42	2.7	0.22	– 5.98	+2.79	ol	plag	cpx	opx	glass		–[g]	0.38
#77	501.7	1,130 ± 4	42	n.a.	–	–	–	ol	plag	cpx	opx	glass		–[f]	
#78	501.5	1,060 ± 6	64	9.0	1.00	– 5.60	+4.09	ol	cpx	cr-sp	glass			–[f]	0.35
#79	501.5	1,060 ± 6	64	6.3	0.57	– 6.08	+3.60	ol (6.8)	plag (16.1)	cpx (27.4)	cr-sp (1.0)	glass (48.8)		0.01	0.42
#80	501.5	1,060 ± 6	64	n.a.	–	–	–	ol	plag	cpx	opx	mag	glass	–[f]	
#81	501.5	1,060 ± 6	64	n.a.	–	–	–	ol	plag	cpx	opx	mag	glass	–[f]	
#82	503.2	980 ± 10	91	8.8	1.00	– 6.81	+4.05	cpx (6.2)	amph (40.8)	glass (53.0)				0.01	
#83	503.2	980 ± 10	91	n.a.	–	–	–	plag	cpx	opx	amph	mag	glass	–[f]	

ol olivine, *plag* plagioclase, *cpx* clinopyroxene, *opx* orthopyroxene, *cr-sp* Cr-rich spinel, *mag* magnetite, *amph* amphibole

[a]Water content determined the with "by-difference" method (e.g., Devine et al. 1995)

[b]aH_2O calculated after Burnham (1979)

[c]log fO_2 was calculated following the procedure of Scaillet et al. (1995) with values of: Robie et al. (1978; Kw), Pitzer and Sterner (1994; water fugacity), Burnham (1979; water activity), Chou (1987; oxygen buffer, water-saturated) using values of Schwab and Küstner (1981) and Huebner and Sato (1970), Shaw and Wones (1964; hydrogen fugacity)

[d]Phase proportions calculated by mass balance

[e]Calculated after Roeder and Emslie (1970), with Fe^{2+}–Fe^{3+} calculation after Kress and Carmicheal (1991)

[f]At least one phase is too small for reliable analyses

[g]A negative value is calculated for at least one phase

Table 2 Compositions of the experimental phases in wt%, starting material: R6a

Run	Temp. (°C)	Phase	n[a]	SiO_2	TiO_2	Al_2O_3	FeO^{tot}	MnO	MgO	CaO	Na_2O	K_2O	NiO	Cr_2O_3	P_2O_5	Total	X[b]
Starting composition R6a				50.43	0.35	17.18	6.50	0.16	10.12	11.54	2.84	0.04			< 0.03	99.16	
Starting material: R6a (100 MPa)																	
#58	980	ol	4	41.97 (.12)		0.96 (.40)	9.24 (.13)	0.33 (.03)	47.82 (.72)	0.80 (.34)	0.15 (.06)		0.13 (.02)			101.40	90.2 (.1)
		plag	5	53.83 (.24)	0.05 (.01)	28.22 (.29)	1.11 (.12)		0.48 (.28)	12.03 (.19)	4.61 (.17)	0.04 (.00)				100.37	58.9 (.7)
		cpx	6	51.41 (.14)	0.55 (.05)	4.30 (.30)	6.05 (.22)	0.22 (.03)	16.61 (.36)	20.81 (.43)	0.61 (.05)					100.55	83.0 (.7)
		opx	2	55.99 (.04)	0.15 (.00)	7.57 (1.07)	6.34 (.27)	0.26 (.03)	27.74 (.34)	3.32 (.21)	0.80 (.11)					102.18	88.6 (.6)
		glass	n.a.[c]														
#50	1,060	ol	10	41.18 (.19)		0.10 (.11)	11.01 (.10)	0.24 (.05)	48.19 (.31)	0.36 (.11)			0.12 (.06)			101.20	88.6 (.1)
		plag	7	47.02 (.54)	0.04 (.02)	32.42 (.64)	1.12 (.14)		0.40 (.15)	17.04 (.50)	1.74 (.27)					99.78	84.4 (2.4)
		cpx	6	50.59 (.87)	0.29 (.04)	4.98 (.81)	5.69 (.54)	0.11 (.05)	15.53 (.50)	22.30 (.52)	0.37 (.05)			0.49 (.14)		100.34	83.0 (1.7)
		glass	8	51.93 (.44)	0.41 (.04)	18.08 (.15)	6.56 (.33)	0.13 (.10)	5.67 (.13)	10.30 (.17)	3.72 (.18)	0.06 (.02)				96.86	78.4
#51	1,060	ol	7	39.81 (.20)		0.10 (.04)	16.70 (.15)	0.32 (.06)	43.25 (.21)	0.38 (.06)			0.12 (.04)			100.69	82.2 (.2)
		plag	6	51.69 (.38)	0.06 (.02)	29.46 (.28)	1.15 (.07)		0.25 (.05)	13.49 (.27)	3.80 (.08)					99.90	66.2 (.9)
		cpx	6	51.19 (.54)	0.43 (.05)	3.68 (.43)	6.89 (.35)	0.18 (.04)	15.89 (.38)	21.10 (.31)	0.42 (.05)			0.28 (.05)		100.06	80.4 (1.0)
		glass	5	54.83 (.37)	0.80 (.06)	17.00 (.26)	7.57 (.37)	0.11 (.08)	4.36 (.30)	8.39 (.27)	4.80 (.34)	0.12 (.03)				97.98	67.7
#52	1,060	ol	4	40.02 (.59)	0.06 (.03)	1.29 (.63)	20.93 (.63)	0.34 (.07)	37.44 (.92)	1.28 (.62)	0.16 (.07)		0.12 (.05)			101.63	76.1 (.4)
		plag	5	53.40 (.15)	0.11 (.02)	26.60 (.47)	1.40 (.17)		1.56 (.44)	11.55 (.37)	4.55 (.08)	0.04 (.01)				99.22	58.2 (1.1)
		cpx	4	50.72 (1.18)	0.81 (.03)	4.52 (1.73)	8.72 (.75)	0.23 (.02)	16.44 (1.72)	16.93 (1.63)	0.59 (.19)			0.19 (.03)		99.15	77.1 (1.0)
		glass	n.a.[c]														
#53	1,060	ol	5	39.62 (.51)		0.23 (.17)	19.10 (.35)	0.37 (.06)	40.98 (.21)	0.51 (.11)						100.80	79.3 (.3)
		plag	5	53.26 (.44)	0.07 (.02)	27.99 (.47)	1.16 (.09)		0.35 (.22)	12.10 (.23)	4.68 (.16)	0.03 (.01)				99.63	58.7 (1.3)
		cpx	6	51.93 (.37)	0.56 (.05)	3.10 (.36)	7.63 (.27)	0.22 (.05)	16.33 (.34)	20.01 (.36)	0.41 (.03)			0.22 (.03)		100.40	79.2 (.6)
		glass	4	55.28 (.46)	1.01 (.14)	19.55 (.86)	7.42 (.30)	0.16 (.08)	3.53 (.33)	8.85 (.21)	4.71 (.23)	0.12 (.03)				100.65	61.2
#42	1,100	ol	7	41.67 (.18)		0.05 (.03)	7.40 (.13)	0.15 (.05)	51.12 (.24)	0.29 (.02)			0.16 (.05)			100.83	92.5 (.1)
		glass	7	50.05 (.30)	0.34 (.03)	17.51 (.16)	5.96 (.30)	0.18 (.11)	7.54 (.18)	11.74 (.31)	2.90 (.23)	0.03 (.01)				96.26	84.1
#44	1,100	ol	8	39.74 (.19)		0.13 (.06)	17.26 (.23)	0.32 (.02)	42.57 (.19)	0.42 (.04)						100.45	81.5 (.2)
		plag	7	52.84 (.27)	0.05 (.01)	28.43 (.40)	1.04 (.10)		0.37 (.14)	12.46 (.21)	4.12 (.04)	0.02 (.01)				99.31	62.5 (.6)
		cpx	6	52.03 (.20)	0.50 (.04)	3.14 (.12)	7.12 (.17)	0.22 (.05)	16.58 (.23)	19.96 (.40)	0.41 (.03)			0.27 (.03)		100.22	80.6 (.4)
		glass	6	53.96 (.75)	1.11 (.08)	15.98 (.42)	8.57 (.39)	0.15 (.11)	5.25 (.08)	8.57 (.35)	4.23 (.18)	0.14 (.04)				97.96	67.5
#45	1,100	ol	8	40.03 (.14)		0.11 (.06)	15.81 (.27)	0.29 (.06)	43.66 (.24)	0.43 (.04)						100.33	83.1 (.2)
		plag	5	52.32 (.50)	0.06 (.02)	29.10 (.31)	1.09 (.02)		0.34 (.09)	13.17 (.18)	3.88 (.11)	0.02 (.01)				99.98	65.2 (.9)
		cpx	8	51.58 (.35)	0.45 (.05)	3.18 (.25)	7.49 (.30)	0.20 (.06)	16.57 (.22)	19.96 (.41)	0.37 (.04)			0.26 (.05)		100.05	79.8 (.6)
		glass	7	53.86 (.30)	0.88 (.03)	16.08 (.26)	8.16 (.15)	0.16 (.08)	5.42 (.30)	9.16 (.38)	3.93 (.27)	0.10 (.03)				97.75	70.0
#54	1,140	ol	5	41.86 (.07)		0.05 (.03)	6.09 (.22)	0.13 (.02)	52.28 (.08)	0.30 (.03)			0.17 (.07)			100.88	93.9 (.2)
		glass	8	49.90 (.43)	0.36 (.04)	16.98 (.19)	6.06 (.24)	0.12 (.11)	8.83 (.18)	11.49 (.25)	3.04 (.09)	0.05 (.03)				96.83	85.8
#55	1,140	ol	5	41.78 (.26)		0.06 (.02)	8.24 (.17)	0.17 (.04)	50.52 (.26)	0.33 (.02)						101.10	91.6 (.2)
		plag	5	47.32 (.40)		32.22 (.54)	1.01 (.05)		0.46 (.14)	16.89 (.45)	1.89 (.09)					99.79	83.1 (1.0)
		glass	5	50.75 (.15)	0.37 (.06)	17.77 (.23)	6.01 (.21)		7.76 (.12)	12.27 (.17)	3.37 (.28)	0.05 (.05)				98.35	82.1
#56	1,140	ol	6	40.51 (.07)		0.09 (.03)	12.55 (.21)	0.24 (.02)	46.28 (.07)	0.43 (.05)						100.10	86.8 (.2)
		plag	6	51.31 (.30)	0.04 (.03)	29.67 (.54)	1.05 (.16)		0.42 (.18)	14.15 (.30)	3.62 (.08)	0.02 (.01)				100.28	68.3 (.9)
		cpx	7	51.76 (.52)	0.26 (.02)	3.50 (.32)	5.55 (.38)	0.12 (.04)	16.44 (.19)	20.89 (.28)	0.40 (.03)			0.50 (.07)		99.42	84.1 (1.0)
		glass	8	52.74 (.22)	0.62 (.05)	16.06 (.29)	7.86 (.47)	0.18 (.08)	6.43 (.28)	10.75 (.36)	3.76 (.22)	0.07 (.04)				98.47	71.3

Table 2 continued

Run	Temp. (°C)	Phase	n[a]	SiO_2	TiO_2	Al_2O_3	FeO^{tot}	MnO	MgO	CaO	Na_2O	K_2O	NiO	Cr_2O_3	P_2O_5	Total	X[b]
#57	1,140	ol	7	40.51 (.28)		0.06 (.01)	12.92 (.19)	0.25 (.04)	46.22 (.20)	0.43 (.04)						100.39	86.4 (.2)
		plag	7	51.63 (.42)	0.05 (.02)	29.24 (.55)	0.95 (.08)		0.58 (.26)	13.65 (.32)	3.67 (.11)	0.02 (.01)				99.79	67.2 (.9)
		cpx	5	52.03 (.33)	0.31 (.05)	3.30 (.24)	5.73 (.39)	0.17 (.07)	16.94 (.26)	20.42 (.27)	0.36 (.05)			0.37 (.04)		99.63	84.1 (.9)
		glass	7	53.06 (.31)	0.65 (.03)	16.04 (.40)	7.83 (.43)	0.12 (.12)	6.43 (.27)	10.91 (.41)	3.82 (.22)	0.07 (.02)				98.93	72.4
#46	1,160	glass	8	49.70 (.38)	0.31 (.03)	16.79 (.23)	5.57 (.28)	0.15 (.16)	9.80 (.16)	11.44 (.14)	2.72 (.12)	0.05 (.02)			0.06 (.08)	96.59	87.9
#47	1,160	ol	9	41.75 (.21)		0.07 (.02)	7.06 (.30)	0.13 (.03)	51.27 (.33)	0.34 (.04)						100.62	92.8 (.3)
		glass	7	51.03 (.35)	0.39 (.03)	17.53 (.24)	5.34 (.61)	0.13 (.07)	8.86 (.23)	11.81 (.50)	2.78 (.23)	0.05 (.02)			0.06 (.08)	97.98	85.5
#48	1,160	ol	8	41.27 (.21)		0.10 (.09)	8.64 (.33)	0.17 (.05)	49.60 (.42)	0.44 (.08)						100.22	91.1 (.4)
		plag	8	49.54 (.36)		30.64 (.29)	0.67 (.06)		0.48 (.16)	15.19 (.20)	2.79 (.11)					99.31	75.0 (.9)
		cpx	8	51.82 (.31)	0.18 (.01)	3.71 (.17)	3.34 (.23)		17.29 (.28)	22.05 (.21)	0.30 (.03)			1.31 (.07)		100.00	90.2 (.7)
		glass	5	52.79 (.53)	0.42 (.03)	17.38 (.46)	5.56 (.18)	0.14 (.17)	7.73 (.22)	12.20 (.24)	3.30 (.16)	0.05 (.02)				99.57	80.3
#49	1,160	ol	7	41.20 (.17)		0.04 (.02)	8.63 (.22)	0.19 (.03)	49.89 (.26)	0.43 (.04)						100.38	91.2 (.2)
		plag	6	50.95 (.55)	0.05 (.02)	29.67 (.32)	0.73 (.09)		0.59 (.09)	14.35 (.20)	3.27 (.10)					99.61	70.8 (.9)
		cpx	5	52.40 (.04)	0.19 (.02)	3.22 (.33)	3.60 (.29)	0.11 (.03)	17.71 (.21)	21.58 (.14)	0.28 (.01)			0.86 (.15)		99.95	89.8 (.8)
		glass	6	53.98 (.49)	0.47 (.02)	17.11 (.20)	5.23 (.19)	0.15 (.04)	7.57 (.15)	11.73 (.24)	3.35 (.21)	0.06 (.02)				99.65	80.1
#38	1,180	glass	9	49.91 (.38)	0.32 (.03)	16.91 (.20)	6.10 (.17)	0.13 (.04)	9.70 (.20)	11.26 (.20)	2.90 (.19)	0.04 (.03)				97.27	86.6
#39	1,180	ol	9	41.76 (.18)		0.06 (.03)	7.56 (.12)	0.13 (.02)	50.96 (.20)	0.34 (.02)						100.81	92.3 (.1)
		glass	8	51.75 (.20)	0.34 (.02)	17.57 (.23)	5.54 (.17)		9.19 (.19)	12.20 (.23)	2.92 (.18)	0.06 (.02)				99.57	84.3
#40	1,180	ol	9	41.60 (.15)		0.07 (.03)	8.20 (.15)	0.16 (.05)	50.15 (.17)	0.39 (.03)						100.57	91.6 (.1)
		glass	8	51.79 (.22)	0.39 (.04)	17.96 (.27)	5.54 (.22)	0.14 (.08)	8.87 (.23)	12.27 (.20)	3.11 (.26)	0.05 (.03)				100.12	82.9
#41	1,180	ol	9	41.72 (.24)		0.05 (.03)	7.74 (.19)	0.15 (.04)	50.59 (.16)	0.39 (.02)						100.64	92.1 (.2)
		plag	7	50.78 (.40)	0.03 (.02)	29.85 (.29)	0.64 (.05)		0.70 (.13)	14.93 (.35)	3.07 (.17)					100.00	72.8 (1.5)
		glass	10	53.09 (.30)	0.39 (.03)	17.93 (.30)	5.03 (.42)	0.10 (.09)	8.77 (.17)	12.39 (.31)	3.16 (.15)	0.03 (.02)				100.89	82.3
Starting material: R6a (200 MPa)																	
#32	940	plag	7	51.13 (.35)		30.19 (.52)	0.98 (.14)		0.24 (.09)	14.17 (.29)	3.19 (.14)	0.02 (.01)				99.92	71.0 (.7)
		cpx	8	52.33 (.57)	0.15 (.03)	3.24 (.72)	6.81 (.26)	0.30 (.06)	16.97 (1.05)	20.22 (.87)	0.33 (.06)			0.09 (.06)		100.44	81.6 (1.3)
		opx	7	54.73 (.37)	0.06 (.02)	2.83 (.27)	10.89 (.20)	0.40 (.05)	29.84 (.40)	1.41 (.27)						100.16	83.0 (.2)
		glass	8	59.33 (.47)	0.16 (.03)	17.04 (.45)	3.92 (.32)		2.27 (.45)	5.60 (.21)	3.09 (.31)	0.12 (.03)		0.09 (.13)	0.20 (.11)	91.82	70.6
#31	980	ol	5	41.53 (.24)		0.07 (.04)	7.78 (.29)	0.31 (.02)	51.11 (.13)	0.18 (.04)						100.98	92.1 (.3)
		plag	4	48.10 (.37)		32.01 (.28)	1.12 (.19)		0.22 (.05)	16.10 (.10)	2.16 (.14)	0.02 (.00)				99.73	80.4 (1.1)
		cpx	3	51.17 (.08)	0.22 (.03)	4.18 (.33)	6.60 (.21)	0.24 (.05)	17.40 (.39)	20.01 (.33)	0.32 (.04)					100.14	82.5 (.4)
		glass	7	57.13 (.47)	0.26 (.02)	18.07 (.16)	3.62 (.29)	0.11 (.09)	3.49 (.17)	6.56 (.10)	4.27 (.19)	0.10 (.02)			0.11 (.08)	93.72	80.1
#25	1,020	ol	7	41.11 (.23)		0.04 (.04)	10.00 (.62)	0.22 (.08)	48.78 (.56)	0.23 (.03)			0.17 (.04)			100.55	89.7 (.7)
		plag	6	45.80 (.37)		33.43 (.37)	1.13 (.13)		0.20 (.09)	17.84 (.35)	1.50 (.10)					99.90	86.7 (.9)
		cpx	4	50.72 (.44)	0.26 (.01)	4.05 (.56)	5.63 (.33)	0.10 (.03)	16.49 (.22)	22.30 (.59)	0.21 (.18)			0.09 (.03)		99.85	83.9 (.9)
		glass	8	50.26 (.78)	0.41 (.04)	18.14 (.41)	5.78 (.29)		4.49 (.19)	8.87 (.16)	3.62 (.29)	0.06 (.03)			0.05 (.07)	91.68	76.2
#26	1,020	ol	5	39.67 (.19)		0.08 (.02)	16.42 (.34)	0.32 (.04)	42.87 (.20)	0.28 (.03)			0.13 (.04)			99.77	82.3 (.3)
		plag	5	52.44 (.58)	0.08 (.03)	28.45 (.73)	1.24 (.21)		0.51 (.31)	12.73 (.15)	4.43 (.12)	0.02 (.01)				99.90	61.3 (.9)
		cpx	6	50.48 (.67)	0.59 (.06)	4.61 (.80)	7.31 (.19)	0.26 (.04)	15.71 (.38)	20.28 (.44)	0.53 (.04)					99.77	79.3 (.7)
		glass	n.a.[c]														
#10	1,060	ol	10	41.72 (.21)		0.03 (.02)	6.54 (.25)	0.18 (.03)	51.32 (.31)	0.24 (.03)			0.21 (.05)			100.24	93.3 (.3)
		cpx	8	50.77 (.41)	0.17 (.02)	4.08 (.51)	4.56 (.21)	0.10 (.05)	16.20 (.38)	23.03 (.40)	0.25 (.05)			0.35 (.08)		99.51	86.3 (.7)
		glass	11	49.22 (.46)	0.34 (.03)	17.77 (.28)	5.96 (.35)	0.11 (.08)	6.86 (.18)	11.60 (.28)	2.99 (.23)	0.05 (.04)				94.90	82.8

Table 2 continued

Run	Temp. (°C)	Phase	n[a]	SiO_2	TiO_2	Al_2O_3	FeO^{tot}	MnO	MgO	CaO	Na_2O	K_2O	NiO	Cr_2O_3	P_2O_5	Total	X[b]
#11	1,060	ol	9	40.43 (.20)		0.08 (.05)	12.94 (.23)	0.28 (.04)	46.07 (.32)	0.33 (.03)			0.16 (.05)			100.29	86.4 (.2)
		plag	5	50.13 (.38)	0.08 (.04)	28.78 (.48)	1.49 (.24)		0.66 (.23)	13.68 (.10)	3.39 (.14)					98.21	69.0 (.8)
		cpx	9	48.77 (.37)	0.41 (.02)	5.71 (.36)	7.20 (.28)	0.18 (.04)	15.27 (.25)	20.93 (.39)	0.36 (.17)			0.12 (.04)		98.95	79.1 (.5)
		glass	7	53.74 (.39)	0.60 (.06)	17.56 (.21)	7.27 (.26)	0.13 (.09)	4.89 (.09)	8.45 (.30)	4.40 (.21)	0.07 (.03)			0.05 (.05)	97.16	70.2
#12	1,060	ol	3	39.37 (.12)		0.31 (.14)	17.20 (.11)	0.36 (.03)	41.69 (.26)	0.45 (.06)						99.38	81.2 (.1)
		plag	4	52.90 (.19)	0.13 (.05)	27.52 (.37)	1.55 (.32)		0.53 (.10)	11.99 (.22)	4.56 (.09)	0.04 (.00)				99.22	59.1 (.8)
		cpx	7	50.33 (.53)	0.58 (.04)	4.00 (.79)	7.68 (.34)	0.23 (.05)	16.07 (.41)	19.32 (.41)	0.50 (.07)					98.71	78.9 (.6)
		opx	3	53.56 (.70)	0.31 (.03)	4.29 (.30)	11.39 (.43)	0.30 (.03)	26.60 (.23)	2.66 (.30)	0.29 (.05)					99.39	80.6 (.5)
		glass	n.a.[c]														
#13	1,060	ol	3	40.12 (.76)	0.03 (.02)	0.74 (.17)	16.53 (.21)	0.35 (.02)	41.04 (.31)	0.90 (.09)	0.12 (.04)		0.15 (.01)			99.98	81.6 (.1)
		plag	3	52.36 (.12)	0.07 (.03)	27.88 (.23)	1.32 (.12)		0.68 (.19)	12.22 (.16)	4.44 (.10)					98.97	60.2 (.5)
		cpx	5	50.55 (.19)	0.59 (.06)	4.40 (.73)	7.71 (.11)	0.23 (.04)	15.93 (.34)	19.40 (.46)	0.54 (.09)					99.35	78.6 (.3)
		opx	3	53.67 (.59)	0.33 (.03)	5.49 (1.65)	10.63 (.62)	0.29 (.02)	24.98 (1.16)	3.36 (.58)	0.51 (.27)					99.28	80.7 (.2)
		glass	n.a.[c]														
#1	1,100	ol	5	42.06 (.25)		0.05 (.03)	5.51 (.25)	0.16 (.02)	52.92 (.23)	0.22 (.02)			0.27 (.05)			101.19	94.5 (.2)
		glass	11	48.79 (.48)	0.33 (.03)	16.66 (.22)	6.02 (.33)	0.10 (.11)	8.37 (.11)	11.43 (.14)	2.60 (.08)	0.04 (.03)				94.34	85.1
#2	1,100	ol	5	40.83 (.27)		0.04 (.02)	10.71 (.26)	0.27 (.02)	48.77 (.37)	0.28 (.03)						100.91	89.0 (.2)
		plag	5	49.54 (.18)	0.04 (.02)	30.43 (.24)	1.37 (.25)		0.47 (.20)	14.41 (.21)	2.79 (.12)					99.05	74.0 (.9)
		cpx	4	50.55 (.59)	0.29 (.05)	4.74 (.37)	5.87 (.30)	0.16 (.05)	16.14 (.29)	20.78 (.21)	0.35 (.02)			0.45 (.04)		99.34	83.1 (.9)
		glass	7	52.31 (.36)	0.50 (.03)	17.12 (.20)	7.51 (.37)	0.13 (.06)	6.04 (.22)	9.51 (.31)	3.72 (.23)	0.06 (.02)				96.90	73.6
#3	1,100	ol	5	40.17 (.11)		0.11 (.06)	15.34 (.28)	0.28 (.04)	44.76 (.40)	0.38 (.10)			0.13 (.04)			101.16	83.9 (.1)
		plag	5	52.09 (.25)	0.05 (.01)	29.25 (.21)	1.27 (.17)		0.22 (.05)	12.55 (.11)	3.96 (.14)					99.40	63.6 (.8)
		cpx	5	51.27 (.27)	0.38 (.04)	3.85 (.40)	7.16 (.22)	0.20 (.04)	16.45 (.20)	19.41 (.18)	0.44 (.09)			0.26 (.04)		99.42	80.4 (.6)
		glass	8	53.55 (.37)	0.88 (.08)	16.00 (.24)	9.21 (.39)	0.19 (.14)	5.35 (.18)	8.50 (.27)	4.06 (.24)	0.08 (.02)				97.82	64.5
#5	1,100	ol	5	39.84 (.23)		0.27 (.23)	16.92 (.17)	0.33 (.06)	42.90 (.29)	0.46 (.10)						100.71	81.9 (.2)
		plag	6	52.59 (.18)	0.09 (.07)	27.77 (.69)	1.64 (.46)		0.83 (.59)	11.84 (.32)	4.16 (.13)					98.92	61.1 (.9)
		cpx	4	51.45 (.31)	0.47 (.03)	3.43 (.22)	7.67 (.21)	0.24 (.03)	16.61 (.26)	18.99 (.43)	0.42 (.08)			0.25 (.03)		99.54	79.4 (.4)
		glass	6	53.81 (.44)	1.03 (.07)	16.11 (.57)	9.67 (.29)	0.22 (.07)	5.31 (.32)	8.38 (.81)	4.08 (.36)	0.12 (.03)			0.05 (.05)	98.78	62.1
#14	1,140	glass	10	49.12 (.40)	0.33 (.05)	16.57 (.23)	5.87 (.25)	0.14 (.09)	9.16 (.18)	11.21 (.29)	2.74 (.16)	0.05 (.04)				95.19	86.5
#15	1,140	ol	6	41.19 (.31)		0.03 (.02)	7.41 (.09)	0.13 (.02)	51.01 (.22)	0.29 (.03)			0.19 (.03)			100.24	92.5 (.1)
		glass	9	50.73 (.23)	0.35 (.02)	17.56 (.12)	6.20 (.34)	0.11 (.09)	8.22 (.17)	11.76 (.24)	2.89 (.24)					97.82	82.2
#16	1,140	ol	7	40.13 (.19)		0.08 (.04)	12.20 (.23)	0.25 (.07)	46.71 (.13)	0.39 (.03)						99.75	87.2 (.2)
		plag	5	50.75 (.27)	0.03 (.01)	30.13 (.26)	1.01 (.09)		0.41 (.09)	14.49 (.27)	3.28 (.06)					100.09	70.9 (.5)
		cpx	5	51.82 (.40)	0.24 (.02)	4.05 (.30)	5.95 (.20)	0.15 (.05)	17.25 (.39)	20.57 (.36)	0.36 (.00)			0.40 (.03)		100.79	83.8 (.3)
		glass	5	52.84 (.45)	0.56 (.04)	16.59 (.19)	7.81 (.19)	0.16 (.10)	6.65 (.35)	10.86 (.13)	3.67 (.21)	0.07 (.04)			0.07 (.05)	99.28	72.5
#17	1,140	ol	6	39.65 (.19)		0.07 (.02)	13.76 (.12)	0.27 (.05)	45.34 (.28)	0.42 (.04)						99.51	85.5 (.1)
		plag	7	51.06 (.49)	0.04 (.01)	29.54 (.25)	0.97 (.06)		0.36 (.08)	13.53 (.18)	3.87 (.16)					99.36	65.8 (1.1)
		cpx	7	51.52 (.63)	0.34 (.03)	3.78 (.31)	6.91 (.30)	0.20 (.02)	16.95 (.36)	19.79 (.32)	0.40 (.04)			0.38 (.03)		100.28	81.4 (.8)
		glass	5	53.75 (.17)	0.68 (.06)	16.79 (.29)	7.79 (.24)	0.11 (.15)	6.53 (.29)	10.25 (.15)	3.82 (.23)	0.07 (.03)				99.79	71.4
#21	1,160	glass	6	48.17 (.46)	0.33 (.04)	16.26 (.15)	5.89 (.21)	0.10 (.09)	9.29 (.25)	11.31 (.21)	2.70 (.15)	0.02 (.03)		0.12 (.16)		94.19	86.6
#22	1,160	ol	6	41.78 (.13)		0.04 (.01)	7.83 (.13)	0.13 (.05)	50.97 (.22)	0.29 (.04)						101.04	92.1 (.1)
		glass	5	49.56 (.35)	0.34 (.04)	16.78 (.32)	5.68 (.38)	0.14 (.13)	8.52 (.23)	11.68 (.16)	2.92 (.20)				0.06 (.05)	95.68	84.4
#23	1,160	ol	7	41.84 (.30)		0.07 (.02)	8.92 (.19)	0.17 (.04)	49.90 (.10)	0.37 (.03)						101.27	90.9 (.2)
		plag	6	50.71 (.27)		30.71 (.16)	0.75 (.10)		0.38 (.07)	14.97 (.33)	3.28 (.09)					100.80	71.6 (.9)
		glass	7	50.34 (.41)	0.36 (.04)	17.37 (.25)	5.78 (.32)	0.11 (.11)	7.88 (.21)	12.15 (.18)	3.11 (.18)	0.03 (.02)			0.06 (.08)	97.19	80.3

Table 2 continued

Run	Temp. (°C)	Phase	n[a]	SiO_2	TiO_2	Al_2O_3	FeO^{tot}	MnO	MgO	CaO	Na_2O	K_2O	NiO	Cr_2O_3	P_2O_5	Total	X[b]
#24	1,160	ol	7	40.88 (.38)		0.08 (.04)	9.96 (.15)	0.21 (.02)	48.67 (.36)	0.42 (.05)						100.22	89.7 (.2)
		plag	4	51.11 (.44)	0.03 (.01)	30.16 (.21)	0.63 (.03)		0.39 (.04)	14.24 (.05)	3.60 (.04)					100.16	68.6 (.3)
		cpx	6	51.51 (.55)	0.29 (.04)	3.83 (.47)	6.06 (.27)	0.15 (.05)	17.60 (.19)	19.71 (.31)	0.32 (.03)			0.41 (.04)		99.88	83.8 (.6)
		glass	5	52.06 (.46)	0.48 (.04)	16.83 (.09)	5.88 (.24)	0.14 (.09)	7.14 (.07)	11.42 (.17)	3.57 (.31)	0.06 (.05)				97.58	76.4
#6	1,180	glass	8	46.93 (.44)	0.34 (.02)	16.00 (.17)	5.72 (.29)	0.11 (.13)	9.43 (.27)	10.37 (.33)	2.48 (.12)					91.38	86.8
#7	1,180	glass	8	49.11 (.37)	0.35 (.03)	16.64 (.21)	5.69 (.35)	0.10 (.07)	9.66 (.20)	10.77 (.27)	2.72 (.18)	0.03 (.02)				95.06	85.7
#8	1,180	ol	8	41.10 (.18)		0.09 (.09)	7.86 (.11)	0.10 (.05)	50.63 (.22)	0.33 (.03)						100.10	92.0 (.1)
		glass	6	49.66 (.17)	0.35 (.04)	17.13 (.16)	5.61 (.20)	0.11 (.04)	9.21 (.30)	11.20 (.15)	2.98 (.34)	0.03 (.04)			0.05 (.03)	96.34	84.1
#9	1,180	ol	9	41.41 (.21)		0.05 (.01)	6.90 (.16)	0.14 (.03)	51.76 (.22)	0.38 (.02)						100.64	93.0 (.2)
		glass	9	51.70 (.62)	0.34 (.03)	18.10 (.20)	4.60 (.28)		9.10 (.18)	11.95 (.32)	3.00 (.24)					98.78	83.4
#18	1,220	glass	19	50.69 (.44)	0.32 (.04)	17.15 (.25)	6.32 (.23)		9.85 (.12)	11.56 (.29)	2.98 (.22)	0.04 (.03)				98.91	83.0
#19	1,220	glass	17	51.13 (.32)	0.33 (.04)	17.29 (.29)	6.13 (.29)	0.10 (.08)	10.06 (.18)	11.93 (.25)	2.94 (.18)	0.04 (.04)				99.95	82.1
#20	1,220	ol	7	41.42 (.19)		0.07 (.01)	7.22 (.20)	0.13 (.03)	51.50 (.31)	0.36 (.03)						100.70	92.7 (.2)
		glass	16	52.02 (.49)	0.34 (.04)	17.80 (.17)	5.56 (.23)	0.11 (.11)	9.81 (.22)	12.11 (.33)	2.96 (.21)	0.04 (.03)			0.06 (.06)	100.81	81.0
Starting material: R6a (500 MPa)																	
#82	980	cpx	9	47.53 (.37)	0.32 (.03)	7.66 (.28)	7.41 (.25)	0.15 (.05)	13.48 (.23)	23.16 (.16)	0.35 (.03)			0.11 (.04)		100.17	76.4 (.8)
		glass	16	51.54 (.32)	0.22 (.03)	19.02 (.26)	4.42 (.31)	0.14 (.09)	4.08 (.19)	8.71 (.24)	2.99 (.23)	0.05 (.02)				91.17	78.5
#83	980	plag	6	52.58 (.15)		29.62 (.20)	0.90 (.06)		0.15 (.05)	12.82 (.14)	4.16 (.09)	0.02 (.00)				100.25	62.9 (.3)
		cpx	6	50.14 (.26)	0.31 (.03)	5.38 (.22)	7.71 (.17)	0.25 (.03)	14.77 (.17)	20.70 (.18)	0.65 (.02)					99.91	77.3 (.5)
		opx	8	53.81 (.40)	0.09 (.01)	4.24 (.26)	10.70 (.22)	0.29 (.04)	29.78 (.26)	1.23 (.15)	0.06 (.02)					100.20	83.2 (.3)
		glass	n.a.[c]														
#78	1,060	ol	9	41.94 (.32)			6.43 (.16)	0.17 (.04)	51.30 (.17)	0.21 (.04)			0.22 (.06)			100.27	93.4 (.2)
		cpx	6	51.13 (.42)	0.16 (.02)	4.10 (.43)	4.21 (.22)		15.94 (.32)	23.56 (.21)	0.26 (.02)			0.71 (.07)		100.07	87.1 (.8)
		glass	10	48.02 (.30)	0.33 (.03)	16.71 (.22)	5.91 (.16)		7.26 (.10)	11.33 (.26)	2.65 (.20)	0.10 (.02)				92.31	83.2
#79	1,060	ol	8	40.40 (.20)		0.06 (.04)	12.49 (.28)	0.20 (.03)	46.81 (.24)	0.23 (.05)			0.13 (.04)			100.32	87.0 (.2)
		plag	6	49.22 (.41)	0.03 (.01)	31.30 (.33)	0.97 (.05)		0.24 (.05)	14.18 (.28)	2.86 (.17)	0.02 (.01)				98.83	73.3 (1.5)
		cpx	7	48.63 (.36)	0.35 (.03)	7.09 (.42)	7.01 (.23)	0.15 (.03)	14.99 (.31)	19.24 (.50)	0.51 (.02)			0.16 (.07)		98.13	79.1 (.4)
		glass	10	51.55 (.57)	0.44 (.05)	19.20 (.39)	6.32 (.42)	0.11 (.10)	5.19 (.15)	7.67 (.23)	4.31 (.21)	0.06 (.02)				94.84	73.9
#80	1,060	ol	3	40.01 (.37)	0.04 (.02)	0.59 (.41)	16.91 (.03)	0.40 (.05)	41.98 (.64)	0.52 (.20)	0.07 (.08)					100.52	81.6 (.2)
		plag	4	54.06 (.26)	0.06 (.01)	27.97 (.42)	0.99 (.09)		0.43 (.13)	11.68 (.07)	4.72 (.07)	0.05 (.02)				99.96	57.8 (.4)
		cpx	7	50.38 (.24)	0.65 (.04)	5.05 (.17)	8.03 (.28)	0.24 (.05)	15.48 (.19)	19.48 (.30)	0.73 (.03)					100.04	77.5 (.6)
		opx	6	53.40 (.35)	0.27 (.02)	4.29 (.15)	12.10 (.21)	0.29 (.06)	28.10 (.38)	1.59 (.16)	0.08 (.05)					100.12	80.6 (.4)
		glass	n.a.[c]														
#81	1,060	ol	1	39.98		0.21	16.87	0.27	42.82	0.34	0.04					100.53	81.9
		plag	5	54.84 (.28)	0.07 (.03)	27.96 (.18)	0.96 (.14)		0.14 (.06)	11.03 (.23)	5.20 (.11)	0.05 (.01)				100.25	54.0 (.9)
		cpx	8	50.13 (.38)	0.69 (.06)	5.59 (.22)	8.16 (.15)	0.21 (.04)	15.10 (.27)	19.45 (.34)	0.79 (.08)					100.12	76.8 (.3)
		opx	n.a.[d]														
		glass	n.a.[c]														
#70	1,100	ol	24	42.26 (.17)			5.55 (.14)	0.14 (.04)	52.52 (.18)	0.17 (.02)			0.32 (.06)			100.96	94.4 (.1)
		glass	18	47.93 (.40)	0.34 (.05)	16.14 (.27)	5.98 (.31)	0.10 (.11)	9.12 (.16)	11.02 (.22)	2.47 (.18)	0.17 (.04)				93.27	85.7
#71	1,100	ol	8	40.02 (.16)		0.15 (.11)	15.79 (.27)	0.28 (.04)	43.45 (.39)	0.35 (.05)						100.04	83.1 (.3)
		plag	5	52.34 (.45)	0.04 (.02)	29.59 (.26)	0.89 (.13)		0.19 (.07)	12.88 (.13)	4.22 (.09)	0.02 (.01)				100.17	62.7 (.7)
		cpx	6	50.90 (.29)	0.39 (.04)	4.97 (.38)	7.48 (.16)	0.19 (.07)	16.10 (.24)	19.10 (.21)	0.55 (.05)			0.22 (.05)		99.90	79.3 (.5)
		opx	6	54.21 (.69)	0.14 (.04)	3.47 (.76)	10.90 (.19)	0.25 (.06)	29.18 (.37)	1.74 (.07)	0.07 (.02)			0.12 (.03)		100.08	82.7 (.4)
		glass	6	52.66 (.27)	0.80 (.05)	17.76 (.15)	8.22 (.32)	0.20 (.12)	5.22 (.14)	8.04 (.22)	4.29 (.18)	0.11 (.02)				97.30	66.1

Table 2 continued

Run	Temp. (°C)	Phase	n^a	SiO_2	TiO_2	Al_2O_3	FeO^{tot}	MnO	MgO	CaO	Na_2O	K_2O	NiO	Cr_2O_3	P_2O_5	Total	X^b
#72	1,100	ol	6	39.84 (.26)		0.12 (.13)	17.09 (.19)	0.26 (.04)	42.99 (.21)	0.33 (.07)						100.63	81.8 (.2)
		plag	6	52.91 (.30)	0.04 (.01)	29.33 (.09)	0.86 (.04)		0.17 (.03)	12.53 (.10)	4.39 (.08)	0.02 (.01)				100.25	61.1 (.5)
		cpx	5	50.89 (.28)	0.44 (.04)	4.89 (.16)	8.39 (.31)	0.20 (.04)	16.36 (.23)	18.10 (.48)	0.59 (.04)			0.17 (.05)		100.03	77.7 (.6)
		opx	7	53.53 (.44)	0.20 (.02)	4.20 (.42)	12.16 (.28)	0.30 (.04)	28.42 (.18)	1.77 (.08)	0.07 (.02)			0.12 (.03)		100.77	80.6 (.4)
		glass	7	52.62 (.65)	0.95 (.06)	17.71 (.24)	8.66 (.25)	0.12 (.13)	5.14 (.13)	7.74 (.21)	4.56 (.28)	0.15 (.04)				97.65	63.3
#73	1,100	ol	6	39.67 (.14)	0.03 (.01)	0.14 (.07)	18.75 (.50)	0.32 (.04)	41.82 (.16)	0.38 (.08)						101.11	79.9 (.5)
		plag	6	53.32 (.23)	0.04 (.03)	28.96 (.25)	1.05 (.10)		0.21 (.11)	12.12 (.16)	4.56 (.04)	0.03 (.01)				100.29	59.4 (.4)
		cpx	7	50.09 (.39)	0.61 (.05)	5.25 (.40)	8.60 (.32)	0.25 (.04)	15.56 (.22)	18.63 (.26)	0.63 (.03)			0.16 (.07)		99.78	76.3 (.8)
		opx	3	53.97 (.50)	0.30 (.08)	4.95 (1.54)	11.95 (.14)	0.27 (.05)	26.31 (1.35)	2.63 (.29)	0.26 (.12)	0.02 (.01)				100.66	79.7 (.7)
		glass	n.a.[c]														
#74	1,130	glass	11	47.51 (.26)	0.32 (.04)	15.85 (.16)	5.94 (.40)	0.11 (.09)	9.16 (.18)	10.88 (.28)	2.30 (.18)	0.29 (.05)				92.36	85.8
#75	1,130	ol	10	41.90 (.25)		0.06 (.06)	7.04 (.08)	0.16 (.03)	51.04 (.28)	0.26 (.04)			0.18 (.05)			100.64	92.8 (.1)
		cpx	9	50.13 (.38)	0.18 (.03)	5.89 (.50)	4.80 (.32)		16.10 (.26)	21.37 (.39)	0.41 (.04)			0.80 (.22)		99.68	85.7 (.8)
		glass	18	49.86 (.45)	0.36 (.03)	17.57 (.21)	6.10 (.34)		8.14 (.18)	11.34 (.27)	3.01 (.22)	0.04 (.02)				96.42	81.5
#76	1,130	ol	7	40.43 (.10)		0.08 (.05)	13.72 (.16)	0.26 (.04)	45.54 (.21)	0.29 (.03)						100.32	85.5 (.2)
		plag	4	52.32 (.12)	0.03 (.01)	29.21 (.31)	0.97 (.09)		0.22 (.03)	12.74 (.14)	4.09 (.10)	0.02 (.01)				99.60	63.2 (.6)
		cpx	5	50.11 (.35)	0.36 (.03)	5.48 (.33)	7.28 (.25)	0.16 (.04)	16.15 (.28)	19.01 (.69)	0.52 (.04)			0.31 (.05)		99.38	79.8 (.6)
		opx	1	53.70	0.11	4.44	9.90	0.14	29.90	1.84	0.06			0.15		100.24	84.3
		glass	10	52.10 (.36)	0.70 (.05)	17.48 (.22)	8.16 (.26)	0.17 (.08)	6.27 (.24)	8.82 (.24)	4.01 (.23)	0.08 (.04)			0.05 (.06)	97.84	69.0
#77	1,130	ol	6	39.62 (.20)		0.10 (.05)	16.53 (.22)	0.30 (.04)	42.62 (.30)	0.35 (.02)						99.52	82.1 (.3)
		plag	4	52.69 (.32)	0.07 (.01)	28.62 (.53)	1.02 (.13)		0.30 (.14)	12.39 (.20)	4.51 (.03)	0.04 (.00)				99.64	60.1 (.4)
		cpx	6	50.67 (.65)	0.50 (.06)	4.91 (.50)	8.48 (.24)	0.26 (.06)	16.34 (.64)	17.60 (.58)	0.55 (.03)			0.20 (.06)		99.51	77.5 (.7)
		opx	6	52.79 (.39)	0.24 (.03)	4.29 (.37)	12.04 (.31)	0.26 (.05)	27.84 (.27)	1.92 (.16)	0.08 (.02)			0.13 (.05)		99.59	80.5 (.4)
		glass	n.a.[c]														
#67	1,160	ol	6	41.92 (.20)		0.04 (.02)	6.38 (.10)	0.16 (.03)	51.90 (.20)	0.27 (.03)			0.18 (.06)			100.85	93.5 (.1)
		glass	8	49.66 (.40)	0.35 (.04)	16.76 (.23)	6.15 (.35)		9.30 (.24)	11.23 (.37)	2.88 (.18)	0.04 (.03)				96.37	83.4
#68	1,160	ol	8	42.02 (.13)		0.06 (.05)	6.52 (.10)		51.51 (.11)	0.27 (.03)			0.18 (.03)			100.56	93.4 (.1)
		glass	9	49.95 (.28)	0.33 (.04)	16.67 (.16)	6.10 (.17)	0.12 (.09)	9.35 (.24)	11.51 (.35)	2.85 (.16)	0.03 (.03)				96.91	83.2
#69	1,160	ol	9	40.39 (.24)		0.07 (.01)	14.64 (.23)	0.21 (.09)	44.92 (.18)	0.34 (.03)						100.57	84.5 (.2)
		plag	7	52.96 (.40)	0.05 (.02)	29.01 (.31)	0.87 (.12)		0.37 (.16)	12.90 (.16)	4.23 (.09)	0.02 (.01)				100.41	62.7 (.5)
		cpx	10	51.50 (.40)	0.38 (.05)	4.84 (.42)	7.42 (.37)	0.18 (.05)	17.01 (.39)	18.31 (.68)	0.50 (.03)			0.20 (.05)		100.34	80.3 (.7)
		glass	9	52.70 (.31)	0.81 (.05)	17.46 (.37)	8.52 (.27)	0.20 (.10)	6.29 (.21)	9.24 (.42)	3.92 (.19)	0.09 (.03)				99.23	64.8

Missing values: below detection limit of the electron microprobe

ol olivine, *plag* plagioclase, *cpx* clinopyroxene, *opx* orthopyroxene

[a] Number of analyses; numbers in paratheses are standard deviations (1 σ)

[b] Compositional parameter in mol%: olivine-forsterite content (calculated without MnO); plagioclase–anorthite content (calculated without K_2O); pyroxene $100 \cdot Mg/(Mg + Fe^{2+})$ with Fetot as FeO; glass $100 \cdot Mg/(Mg + Fe^{2+})$ with Fe^{2+} calculated after Kress and Carmicheal (1991)

[c] The glass pools in these runs are too small for reliable analyses

[d] The crystal phase in these runs is too small for reliable analyses

Loss of iron

To avoid iron loss during the experiment Au was used as capsule material at temperatures ≤ 1,020°C. At temperatures > 1,020°C $Au_{80}Pd_{20}$ was used instead of platinum due to its lower Fe solubility (Kawamoto and Hirose 1994). After the experiment, iron loss to the capsule was checked by electron microprobe and found to be negligible, in agreement with previous studies under relatively oxidizing conditions (e.g., Berndt et al. 2005). This conclusion is further supported by the compositions of the iron-bearing phases of the experimental runs. Olivine, for example, systematically increases in forsterite content with temperature and water in the coexisting melt. If iron loss had occurred, an increase in the forsterite content of olivine in runs with low water activities would be expected, which was not observed. Experiments with low water activity and thus low oxygen fugacity could have lost some iron. Mass balance calculations predict iron loss of up to 1.6 wt%, which does not significantly affect the results.

Calculation of water activity and oxygen fugacity

With the help of the estimated water contents of the melts (see below), water activities for each run were calculated according to the model of Burnham (1979). This model works well up to 200 MPa (e.g., Berndt et al. 2005), but is not correct for higher pressures. A correction term was introduced for calculating those water activities for 500 MPa, assuming that the model calculates the relative values for different water contents correctly. Based on this assumption, the water-saturated experiments were defined as $aH_2O = 1$ and the relative deviation, calculated by the model, was subtracted from the experiments performed at the same conditions but with reduced water activity.

The experimental runs were conducted under ''intrinsic'' fO_2 condition of the IHPV, which was measured by Berndt et al. (2002) at four temperatures using solid redox sensor and corresponds to QFM + 4.2 (4.2 log units above the quartz-fayalite-magnetite oxygen buffer) for water saturation. Since the fO_2 in a given run is strongly affected by the water activity (aH_2O; e.g., Berndt et al. 2005; Scaillet et al. 1995) the fO_2 of our experiments varied between ~ QFM + 1.0 for ''nominally dry'' runs (near liquidus) and QFM + 4.2 for water-saturated runs.

The prevailing oxygen fugacity for each experiment with reduced aH_2O was calculated according the procedure outlined by Scaillet et al. (1995). The water fugacity was calculated from aH_2O using the equation of Pitzer and Sterner (1994) with a K_W of Robie et al. (1978). Finally, the oxygen fugacity was determined after Chou (1987) using the values of Schwab and Küstner (1981) and Huebner and Sato (1970) and a fH_2 after Shaw and Wones (1964) which is imposed by the vessel and corresponds to QFM + 4.2 (Berndt et al. 2002).

Difficulties reaching ''dry'' conditions in our experiments

In our ''dry'' experiments, the capsules were dried (as described above) and immediately welded shut. However, Fourier transform infrared (FTIR) measurements of quenched glasses from near-liquidus experiments revealed a water content of these capsules of 0.52 wt%. Experiments with silver oxalate (without added water) also did not reach perfectly ''dry'' conditions. Moreover, these experiments resulted in even higher water contents compared to the procedure described above. We assume that absorbed water due to the hygroscopic character of the silver oxalate is responsible for increasing the water content of the system.

We consider two possible origins of the water in these capsules. First, there is always a certain amount of air in the capsule. The experiments were conducted as a ''closed system'' with the exception of hydrogen (which controls the oxygen fugacity). Hydrogen diffuses through the capsule wall and produces water inside the capsule. Second, the prevailing oxygen fugacity during the experiments is lower compared to the syntheses of the starting material. If so, some of the Fe^{3+} is reduced to Fe^{2+} and the released oxygen forms water with the hydrogen of the buffer.

These ''nominally dry'' experiments (0.52 wt% H_2O) change their water content with the degree of crystallization and can reach water saturation depending on pressure and temperature. In accordance with Berndt et al. (2005), these experiments show a distinct difference to the experiments which are water saturated from beginning on. Berndt et al. (2005) explained this effect by the different amount and composition of crystals and melt. Our experiments fit well with the observation that the bulk water has a significant control. Even at low temperatures, the systematic effect of water on the phase compositions is present (see chapter ''phase chemistry'').

Analytical methods

The products of the experiments were analyzed with a ''Cameca SX100'' electron microprobe equipped with an operating system ''Peak sight'' based on Microsoft

Windows. All data were obtained using 15 kV acceleration potential, a static (fixed) beam, Ka emission from all elements, and a matrix correction according to Pouchou and Pichoir (1991). The minerals were analyzed with a focused beam, 15 nA beam current and counting times of 5 s for Na and K, 30 s for Ni and Cr and 10 s for all other elements. The coexisting glass was measured with a 5 μm defocused beam at 15 kV, 4 nA beam current and counting times of 4 s for Na and K, 30 s for Ni, Cr and P, and 8 s for all other elements. For small glass pools, a beam diameter of 2–5 μm was used. Potential sodium loss was checked by mass balance calculations and found to be negligible.

The water content of the experimental glasses was estimated by the ''by-difference'' method (e.g., Devine et al. 1995). For this, standard glasses of MORB composition with known water contents (published in Berndt et al. 2002) were also analysed during each analytical session.

''Nominally dry'' near liquidus experiments were analysed with an FTIR-spectrometer to determine the minimum water content that was reached in the experiments. For the measurements, sample plates with thicknesses of 175–200 μm (each sample ± 2 μm) were prepared and polished from both sides. Crystal-free glass was located with an optical microscope and analysed with a spot size of ~ 100 × 100 μm (50 scans, 2 cm^{-1} resolution). The measurements were performed in the mid-infrared with a Bruker IFS 88 coupled with an IR-Scope II microscope. The setup of the spectrometer contains an InSb-MCT sandwich narrow range detector, a KBr beamsplitter and a ''globar'' light source. Spectra in the range of 500–5,000 cm^{-1} were recorded and the absorption bands at ~ 3,570 cm^{-1} (attributed to the fundamental OH^- stretching vibration) were used to determine the water content (Leschik et al. 2004; Mandeville et al. 2002) with a density of 2,808 g/l ($\rho = -20.8^{*}c_{water} + 2{,}819$; after Ohlhorst et al. 2001) and an absorption coefficient of 70 (Scholze 1959). We determined a minimum water content for the ''nominally dry'' experiments of ~ 0.52 wt%.

Results

Achievement of equilibrium

Previous studies under similar conditions and compositions using the same IHPV (e.g., Berndt et al. 2005) show that chemical equilibrium is reached after 2–5 h at temperatures > 1000°C and 5–10 h at temperatures of 950–1000°C and water-bearing conditions. The durations of our experiments were 20–91 h (depending on temperature). The following observations suggest that equilibrium was obtained: (1) The newly formed crystals are chemically homogeneous and generally euhedral (Figs. 1, 2). (2) Glasses are also homogeneous (within the counting statistics of the microprobe analyses), irrespective of location within the sample. (3) Glass and crystals are homogeneously distributed along the capsule. (4) Phase compositions vary systematically with intensive variables (e.g., temperature). (5) Mineral-melt and mineral-mineral element partitioning relations are

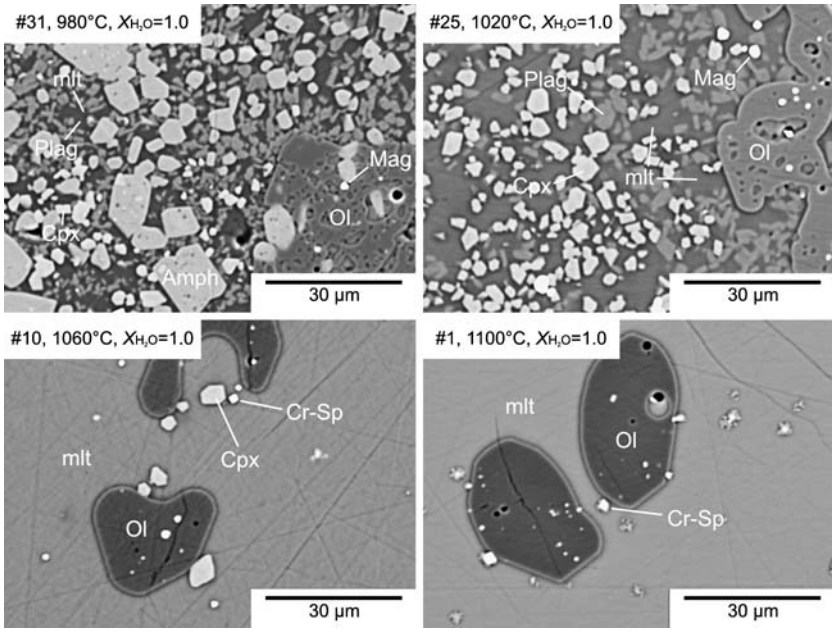

Fig. 1 Back-scattered electron (BSE) images of the experimental products (P = 200 MPa, log fO_2 = QFM + 4.2 and water-saturated conditions). Shown is the effect of temperature on the phase relations. *Ol* olivine, *Cr-Sp* chromium-rich spinel, *Cpx* clinopyroxene, *Plag* plagioclase, *Mag* magnetite, *Amph* amphibole, *mlt* melt

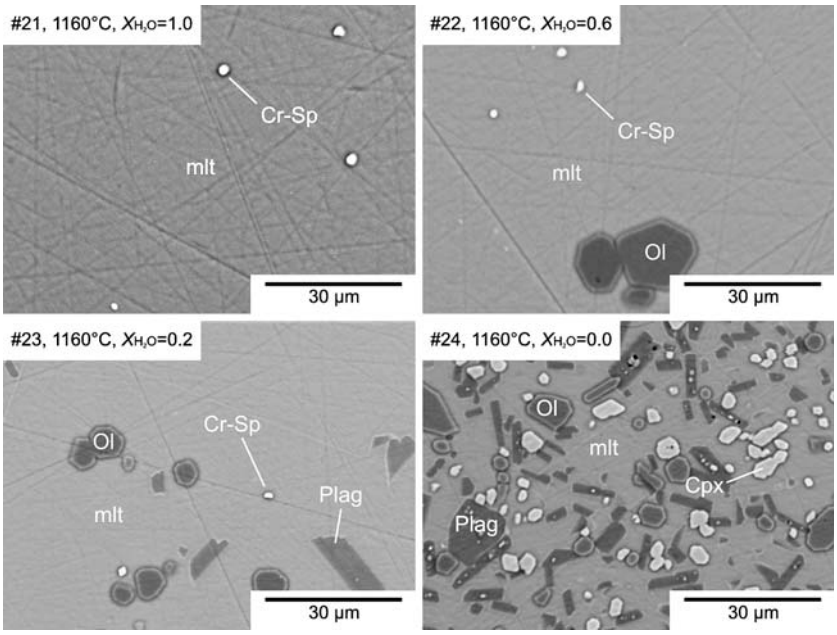

Fig. 2 BSE images of the experimental products (P = 200 MPa, log fO_2 = QFM + 1 – QFM + 4.2 and a temperature of 1,160°C). Shown is the effect of water content on the phase relations. Abbreviations as in Fig. 1

generally in good agreement with published data from other studies (see below). (6) Most mass balance calculations for individual runs result in $\Sigma R^2 < 1$ (ΣR^2 = sum of residual squares, e.g., Albarède and Provost 1977; see also Table 1).

Phase relations

The water content has a large effect on the stabilities of phases in a basaltic system. The addition of water to the dry system shifts the solidus about 250°C to lower temperatures, increases the amount of melt drastically (compare run #1 with #5; 12.5% glass and 96.3% glass respectively) and affects the order of mineral crystallization significantly. The phase relations obtained for 100, 200 and 500 MPa are shown in T – H_2O diagrams (Fig. 3a–c). Experimental conditions and phase proportions are listed in Table 1. At all pressures and water contents, a chrome-rich spinel is the primary liquidus phase, followed by olivine. At lower temperatures, plagioclase and clinopyroxene follow. Their relative order of appearance depends on both pressure and water content. At 100 MPa plagioclase crystallizes before clinopyroxene at all water contents. At pressures above 100 MPa, plagioclase crystallizes before clinopyroxene at low melt water contents (less than ~ 3 wt%), but after clinopyroxene at high water contents, which is in agreement with Gaetani et al. (1993, 1994). The clinopyroxene-saturation curve more or less parallels the olivine-saturation curve at lower temperatures at all pressures and water contents, and the changing of the crystallization order at pressures above 100 MPa is due to a drastic shift of the plagioclase-saturation curve to lower temperatures with increasing water contents (Fig. 3a–c).

Chrome-rich spinel disappears generally after the crystallization of clinopyroxene, suggesting that the Cr content in the melt is lowered by the incorporation of Cr into the clinopyroxene. After a gap of 30 to 100°C, magnetite becomes stable, which reflects the oxidizing conditions in our experiments. At relatively low temperatures, orthopyroxene crystallizes, showing a stability field that depends strongly on the prevailing pressure (see discussion below). Amphibole crystallizes only at temperatures < 1,020°C.

In Fig. 4 we present the phase relations only for the water-saturated conditions, in order to allow comparison with those experimental studies in basaltic systems which were performed exclusively under water-saturated conditions. For example, our 200 MPa water-saturated experiments are in good agreement with the results of Gaetani et al. (1994) for a basaltic andesite at the same pressure.

Figure 4 also illustrates the pressure effect on the liquidus temperatures of the mineral phases. A negligible pressure effect under water-saturated conditions is observed for clinopyroxene and amphibole. Olivine and chromium-rich spinel show a slight decrease in liquidus temperature with increasing pressure, whereas plagioclase, magnetite and orthopyroxene show a strong decrease in liquidus temperature with increasing pressure.

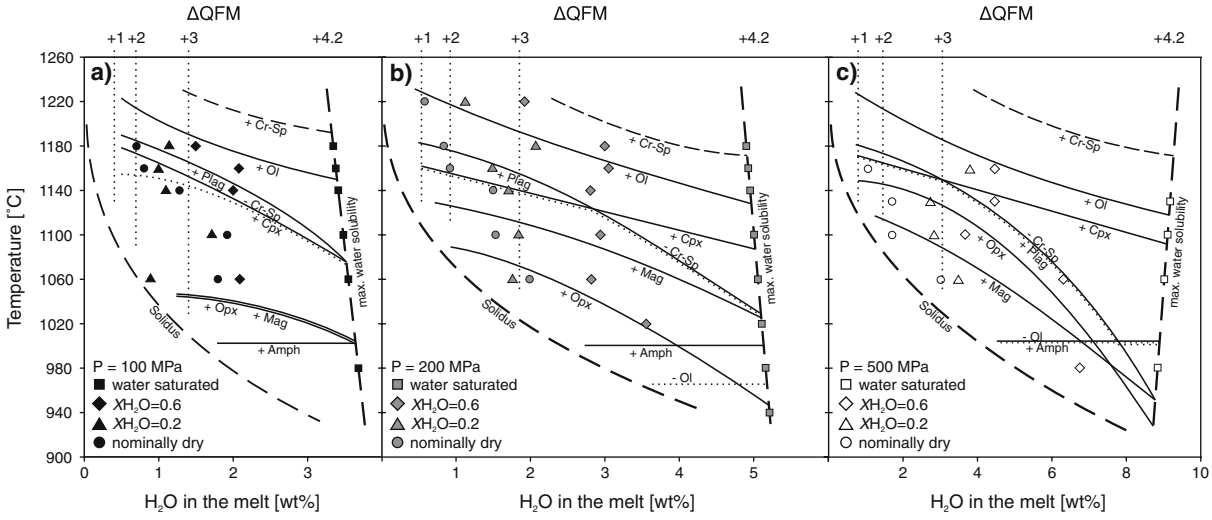

Fig. 3 Phase relations for a hydrous tholeiitic basalt for 100 (**a**) 200 (**b**) and 500 (**c**) MPa. The water-saturation curve included in the phase diagrams is obtained from the water solubility in a primitive MORB of Berndt et al. (2005) and from the temperature and pressure dependence on water solubility by Holtz et al. (1995). The amount of water was determined with the "by-difference" method. Depending on the water activity, the oxygen fugacity (*dotted vertical lines*) varies between QFM + 1 and QFM + 4.2. The symbols represent the experimentally investigated conditions. The total pressure is shown by the *filling* of the symbol; the water content is shown by the *shape* of the symbol. The phase boundaries correspond to the appearance (+) and disappearance (-, *dotted*) of phases. *Ol* olivine, *Cr-sp* chromium-rich spinel, *Cpx* clinopyroxene, *Opx* orthopyroxene, *Plag* plagioclase, *Mag* magnetite, *Amph* amphibole

Phase chemistry

Olivine

Olivine (ol) compositions are listed in Table 2. Figure 5 shows a dramatic increase of forsterite (Fo) component in olivine with increasing water in the system. For instance, at T = 1,100°C the increase of Fo content between "nominally dry" and water-saturated runs is ~12 mol% (at 200 MPa). This effect can partly be ascribed to the increase in melt fraction due to water, and partly to the increase of oxygen fugacity, which is a direct consequence of increasing water activities in a H_2-buffered system. The oxygen fugacity controls the Fe^{2+} content and therefore, the Fe^{2+}/Mg ratio of the melt (e.g., Berndt et al. 2005; Toplis and

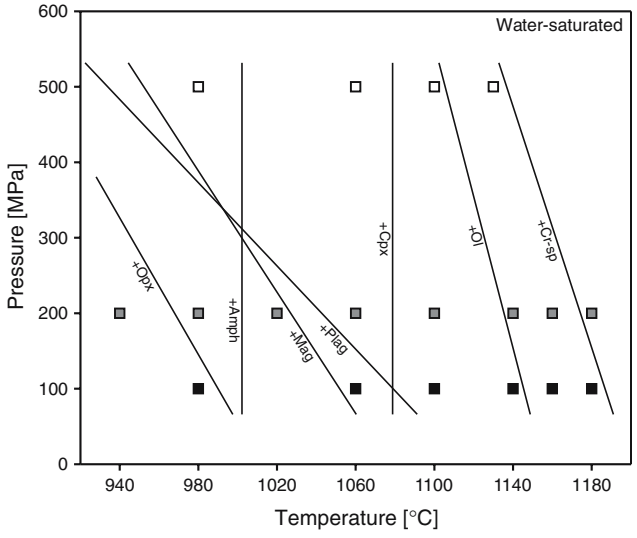

Fig. 4 Liquidus temperatures of the occurring mineral phases as a function of pressure under water-saturated conditions. The *symbols* represent the experimentally investigated conditions. *Ol* olivine, *Cr-sp* chromium-rich spinel, *Cpx* clinopyroxene, *Opx* orthopyroxene, *Plag* plagioclase, *Mag* magnetite, *Amph* amphibole

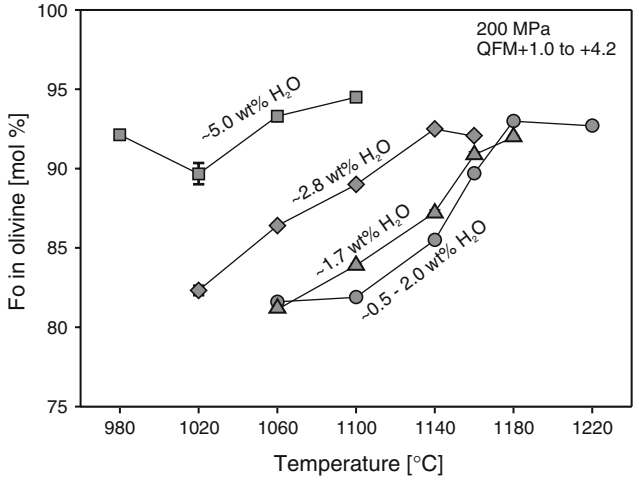

Fig. 5 Forsterite content of olivine as a function of temperature for different water contents at 200 MPa. The signature of the *symbols* is described in Fig. 3

Carroll 1995). For the example from above, the increase in fO_2 correspond to ~ 1.4 log units (Table 1). In Fig. 5 it can be observed that the Fo content tends to rise again at low temperatures, which is due to the crystallization of magnetite extracting FeO from the melt. The same effect was reported in the experiments in a primitive MORB system from Berndt et al. (2005) and is a characteristic of oxidizing conditions.

The element partitioning coefficient $K_{D\ Fe-Mg}^{Ol-Melt}$ according to Roeder and Emslie (1970) was calculated using Eq. 1.

$$K_{D\ Fe-Mg}^{Ol-Melt} = \frac{X_{FeO}^{Ol}}{X_{FeO}^{Melt}} \frac{X_{MgO}^{Melt}}{X_{MgO}^{Ol}} \text{ in mole} \quad (1)$$

The Fe^{2+}/Fe^{3+} ratio of the glass was calculated after Kress and Carmichael (1991). The $K_{D\ Fe-Mg}^{Ol-Melt}$ values obtained for our experiments vary between 0.3–0.47 (Table 1), deviating systematically from the canonical value of Roeder and Emslie (1970) of ~ 0.3 with the amount of water in the system. Toplis (2005) showed that deviations from this value can be expected, mainly due to the influence of melt composition, but also due to water. Values calculated with the model of Toplis (2005) produce $K_{D\ Fe-Mg}^{Ol-Melt}$ values of 0.3 ± 0.01, independent of the prevailing water content.

Plagioclase

Plagioclase compositions are listed in Table 2. Figure 6 shows the strong influence of water on the anorthite content (An) in plagioclase. For instance, at a given temperature of 1,020°C the increase of An between a run with a moderate bulk water content of 2.8 wt% and a water-saturated run is ~ 25 mol% (at 200 MPa). This dramatic increase of An contents due to a higher water content is in full agreement with previous studies (e.g., Berndt et al. 2005; Koepke et al. 2004; Martel et al. 1998; Panjasawatwong et al. 1995).

Clinopyroxene

The clinopyroxene (cpx) compositions are listed in Table 2. Water shifts the Mg# to higher values, as described above for the forsterite content of olivine, and for the same reasons. An effect of water itself on the composition of the pyroxenes cannot be distinguished from the effects mentioned before. In the pyroxene quadrilateral (Fig. 7) the experimental low Ca- and high Ca-pyroxene pairs plot on parallel tie-lines suggesting equilibrium conditions (Lindsley, 1983). As a consequence of the effect of water described above, the experiments show a systematic shift to lower ferrosilite component with increasing water activity.

In Fig. 8 only clinopyroxenes of those runs with the lowest aH_2O for the three different pressures are plotted, displaying well-developed trends for Mg# and some minor components against temperature. It should be mentioned that the water contents of the nominally dry experiments used are not constant, causing some variations within individual trends. As expected, temperatures correlate positively with Mg#, but negatively with TiO_2 and Na_2O, apparently reflecting compositional effects due to higher activities of these components in the melt with decreasing temperature. Figure 8b shows the well-known pressure dependence

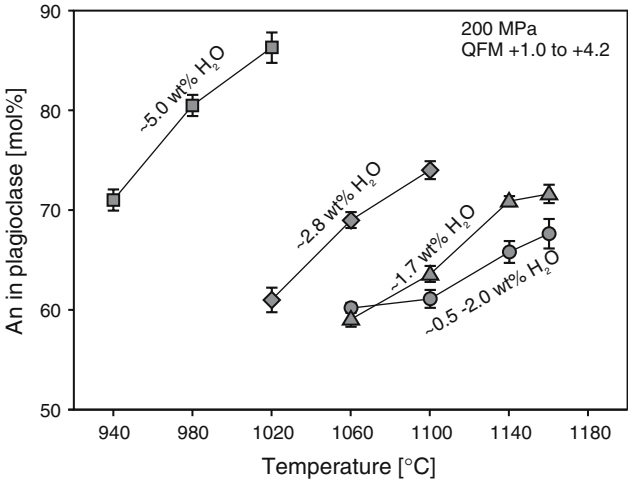

Fig. 6 Anorthite content of plagioclase as a function of temperature for different water contents at 200 MPa. The signature of the *symbols* is described in Fig. 3

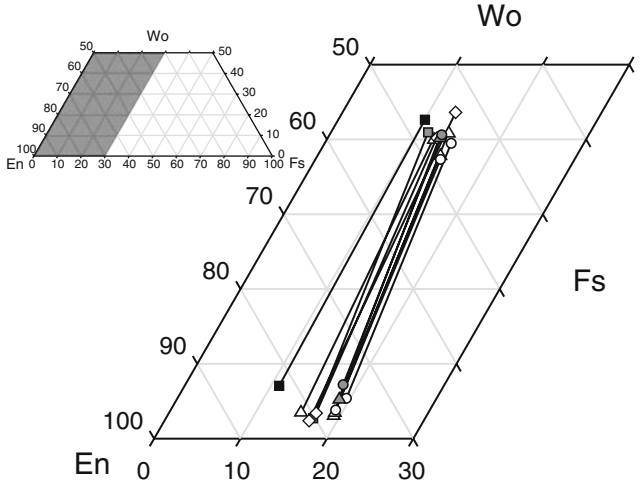

Fig. 7 Pyroxene quadrilateral and the experimental low Ca- and high Ca-pyroxene pairs. Coexisting pyroxenes are connected with tie-lines. The signature of the *symbols* is described in Fig. 3

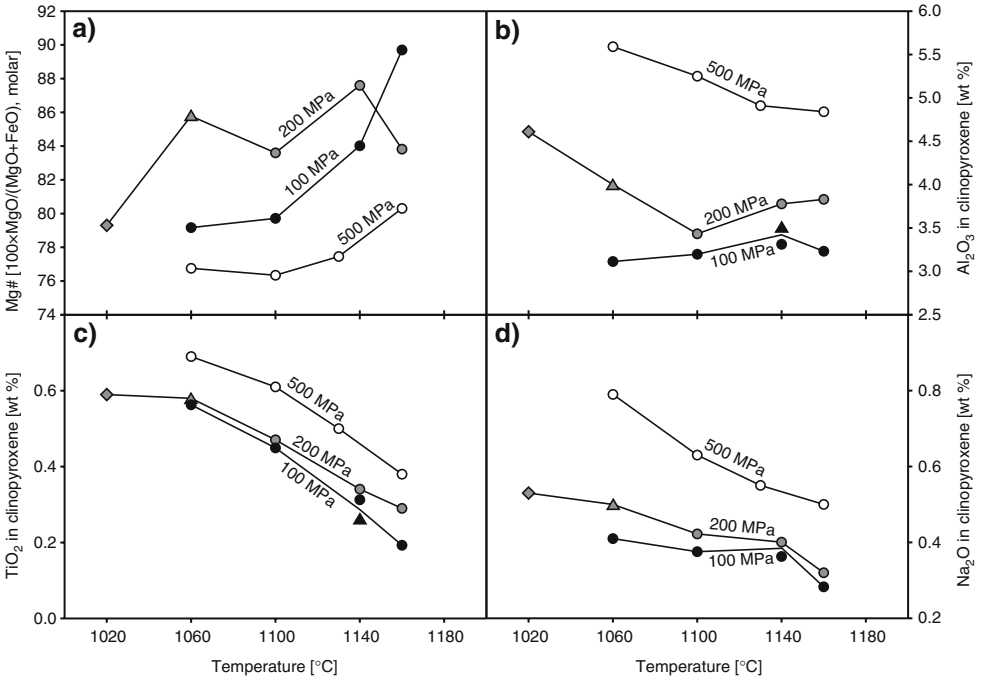

Fig. 8 Mg# and selected components of the clinopyroxenes of the experiments with the lowest water content for the three different pressures as a function of temperature. The signature of the *symbols* is shown in Fig. 3

of Al_2O_3 in clinopyroxene at more or less constant temperatures. The observed trends confirm the potential of clinopyroxene composition for thermobarometry (e.g., Putirka et al. 1996; Putirka et al. 2003) in dry systems.

The well-developed trends for low water contents displayed in Fig. 8 are destroyed when experimental data obtained at higher water contents are included. For clarity, these data points are left out of Fig. 8. This has consequences for applying thermobarometry to clinopyroxene compositional data of hydrous systems. For instance, Putirka et al. (2003) provided a commonly used model to calculate pressures and temperatures using the melt and clinopyroxene composition. We applied their model to our experiments and were able to reproduce the experimental pressures for those runs with low aH_2O well (± 130 MPa) at least for temperatures ≥ 1,100°C, but failed for those runs with high aH_2O (Fig. 9). The temperature dependence shows a systematic deviation from the experimental values to higher temperatures with increasing water activity (Fig. 10).

Orthopyroxene

The orthopyroxene (opx) compositions are listed in Table 2. In contrast to clinopyroxene, orthopyroxene is very sensitive both to total pressure and aH_2O. From 100 to 500 MPa, its saturation curve is shifted by ~ 100°C to higher temperatures at low aH_2O. Due to the limited experiments containing orthopyroxene, clear systematic trends for low and high aH_2O cannot be obtained. Since the Mg# of orthopyroxene correlates well with the Mg# of the associated clinopyroxene (within ~ 5 mol%; see also Fig. 7) both for high and low aH_2O, we infer that increasing melt fraction and fO_2 caused by increasing aH_2O, leads to a shift of Mg# to higher values, analogous to clinopyroxene and olivine. The orthopyroxene with the highest Mg# (88.6) is derived from a run performed under water saturation at a remarkably low temperature of 980°C (#58).

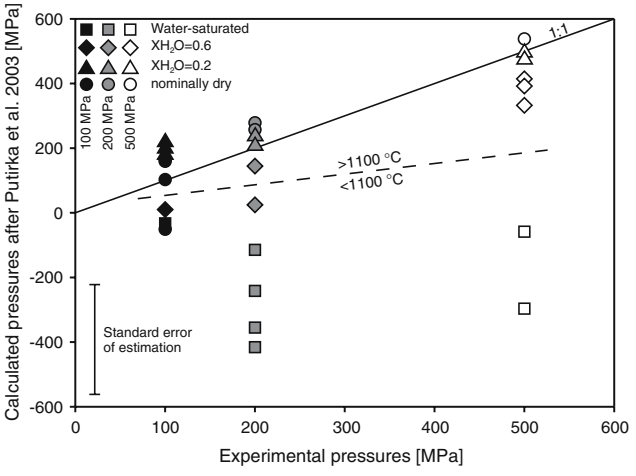

Fig. 9 Thermobarometer of pyroxenes from Putirka et al. (2003) was used to calculate the pressures of the experiments. At high temperatures the calculated pressures reproduce the experimental pressures within the error of the model, at temperatures < 1,100°C the error increases rapidly

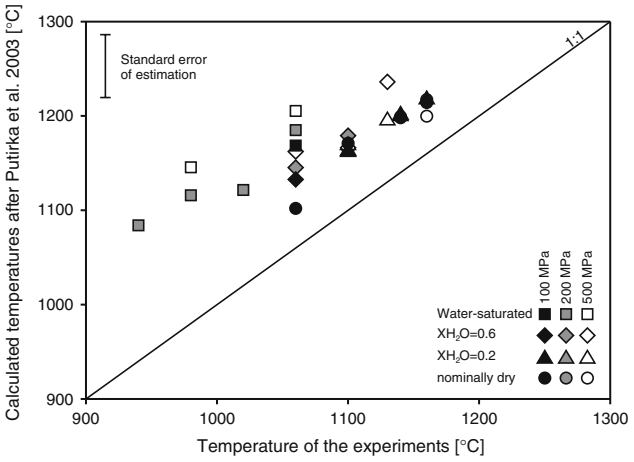

Fig. 10 Thermobarometer of pyroxenes from Putirka et al. (2003) was used to calculate the temperature of the experiments. All pyroxene-bearing experiments show a systematic deviation from the 1:1-line to higher temperatures with increasing water activity in the system

Fe–Ti–Cr–Al oxides

We observed both chromite and magnetite as spinel phases in our experiments, forming tiny crystals often too small for reliable electron microprobe analysis (compositions are presented in the electronic supplementary material only). Chromite typically crystallized at high temperatures and magnetite is the only stable oxide phase at low temperatures. The experimental chromites show compositions typical for those in MORB's and oceanic gabbros (e.g., Rollinson et al. 2002), ranging in composition between Cr#31-56 [Cr# = Cr/(Cr + Al)] and Mg#72-83. At 200 and 500 MPa for high aH_2O chromite and magnetite obviously form solid solutions. For low aH_2O at these pressures and at 100 MPa for all water contents both spinels show distinct stability fields separated by a temperature gap. However, due to the close relationship between water activity and oxygen fugacity in our experiments, it is not possible to trace back the observed compositional trends affected by water to either aH_2O or fO_2. Ilmenite was not observed in our experiments, probably due to the low TiO_2 content of the system. Due to the oxidizing conditions in our experiments, the ulvöspinel component of magnetite is high, ranging between 1.3 and 15.4 mole% (calculated after Stormer 1983).

Amphibole

The amphiboles are pargasite-hastingsite solid solutions (classification after Leake et al. 1997; compositions are presented in the electronic supplementary material only) and are stable at all three pressures at temperatures below 1,020°C. Due to the limited experimental products containing amphibole, systematic trends cannot be obtained. At 200 MPa amphibole crystallized at 980°C show higher tetrahedral Al and Na on the A-site as an amphibole formed at 940°C, which is in agreement with previous experimental studies (Blundy and Holland 1990; Ernst and Liu 1998; Koepke et al. 2004; Sisson and Grove 1993a). When applying the experimental amphibole compositions to the hornblende-plagioclase geothermometer of Blundy and Holland (1990), the experimental temperatures can be reproduced well (experiment#31 and#32 within 20°C; #58 and #83 within 40°C).

Glass compositions

The effect of water on the evolution of the residual melts (compositions in Table 2) is complex due to the interplay of different effects. First, with increasing pressure we observe a strong depression of the plagioclase-saturation temperatures, caused by the water content affecting the plagioclase component in the melt. Second, since our experiments are performed under H_2-buffered conditions, water shifts the oxygen fugacity drastically to higher values, affecting mainly the MgO/FeO ratio in the melt and the stability of magnetite and mafic minerals and their compositions. This leads in general to significantly lower FeO contents in water-rich melts in comparison to dry melts at a given temperature. One consequence of this is that water can change the differentiation trend from ''tholeiitic'' to ''calc-alkaline'' as shown by Berndt et al. (2005) for a primitive MORB system. Third, water not only delays the crystallization of the minerals, it affects also their compositions and consequently the composition of the coexisting liquids. The effect of water on the liquid lines of descent obtained from our experiments performed at 200 MPa is shown in Fig. 11 where the concentration of selected elements in the melt is plotted versus melt fraction. We did this because water shifts the crystal-saturation curves to significantly lower temperatures. This increases the melt fraction considerably, which affects in turn the melt composition, preventing the adequate evaluation of the effect of water on melt compositions in temperature-related plots.

From Fig. 11a it can be inferred that water forces the melt to higher silica contents. The residual melt compositions range from ''primitive'' basaltic to evolved melts approaching the composition of tonalites. Such silicic melts were only observed in water-saturated experimental runs. MgO contents of the residual glasses decrease rapidly with decreasing glass

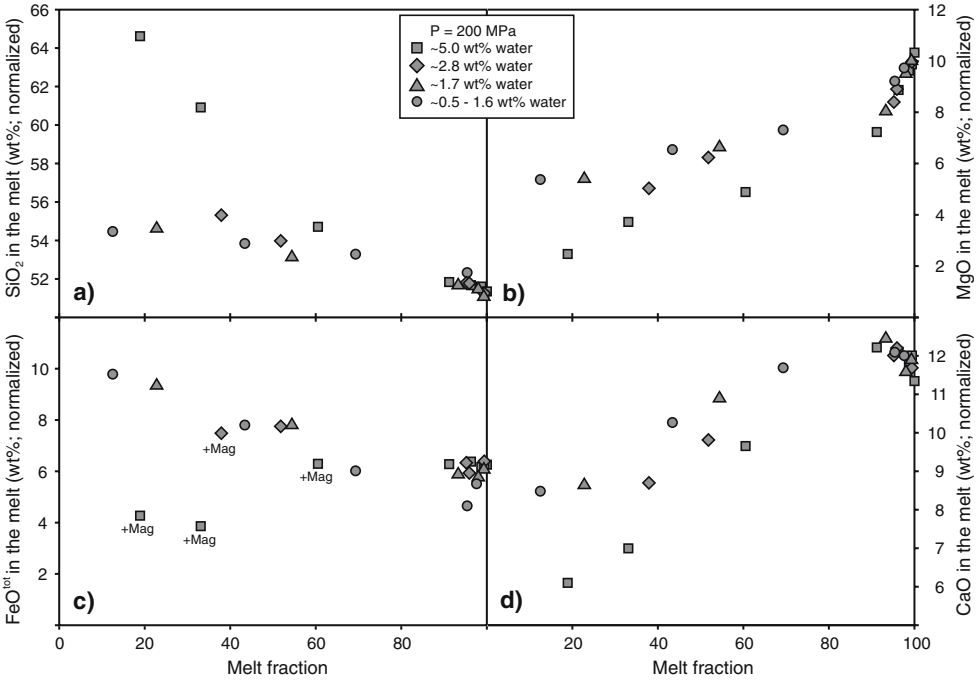

Fig. 11 Selected components of the experimental melts as a function of the melt fraction, calculated by mass balance, for different water contents at 200 MPa. *Mag* magnetite

fraction, due to the crystallization of spinel and olivine at high temperatures (Fig. 11b). Because of the delayed plagioclase crystallization and the increased forsterite contents in olivine due to the higher oxygen fugacity, water shifts the MgO content of the melt to lower values. The FeO^{tot} content of the melt is shown in Fig. 11c. In an early evolution state, the iron content remains more or less constant and is thus not significantly affected by the crystallization of spinel and olivine. FeO^{tot} content in the melt starts to increase with the crystallization of plagioclase. In the low temperature experiments at high water contents, significant amounts of magnetite crystallize resulting in a downward trend. High iron contents in the melts were only reached at reduced water activities. During early crystallization CaO increases in the residual melts (Fig. 11d) due to the negligible CaO contents in the liquidus minerals spinel and olivine. When plagioclase and clinopyroxene starts to crystallize, CaO in the melt decreases rapidly. Due to the strong effect of water on the plagioclase composition, the CaO content of the melt shows a characteristic shift in the trends for the different water contents to lower CaO values.

Discussion

The stability of orthopyroxene in oceanic gabbros

Knowledge of the stability of orthopyroxene in experimental MORB systems is important, since the genesis of oceanic plutonic rocks containing primary orthopyroxene is still under debate (e.g. gabbronorites in the Oman ophiolite or at the Mid-Atlantic Ridge, Boudier et al. 2000; Nonnotte et al. 2005; Shipboard Scientific Party 2004). From experimental studies it is well known that the stability field of orthopyroxene is increased by (1) higher silica activities and (2) by higher pressures of crystallization.

(1) Our experiments show that the silica activity at crustal pressures of our primitive tholeiitic basalt is probably not high enough to produce near liquidus orthopyroxene under dry conditions. In the experiments, orthopyroxene always crystallizes late, at relatively low temperatures (Fig. 3). Even at 500 MPa, where the stability of orthopyroxene is enlarged (under nominally dry conditions), the system has to crystallize more than 66 wt%, before the first orthopyroxene is formed. This implies that the formation of typical gabbronoritic cumulates by simple crystal fractionation seems unlikely. At least one or two fractionation steps are necessary to increase the silica activity in the residual melt (see also Berndt et al. 2005). This is in accord with observations in natural gabbros from the Oman ophiolite where Boudier et al. (2000) found that in a given crustal section typical gabbronorites do not differ chemically from olivine gabbros, except a characteristic SiO_2 enrichment in the former.

(2) The experiments show that the stability of orthopyroxene is significantly affected by the crystallization pressure (Fig. 12). Under nominally dry conditions the orthopyroxene-saturation curve is significantly shifted to higher temperatures (~100°C for a pressure shift from 100 to 500 MPa), whereas under water-saturated conditions, the opposite trend is observed. Thus, pressure enhances the orthopyroxene stability significantly, but only under dry conditions. This is in accord with studies of gabbronorites from the Mid-Atlantic Ridge where pressures up to 800 MPa were considered necessary for the intrusion of gabbroic plutons into the mantle beneath the crust (Shipboard Scientific Party 2004).

The phase diagram in Fig. 12 clearly shows that higher water contents in the melts destabilizes orthopyroxene which could be either the result of a change in melt composition as a function of pressure, water as a chemical component or due the rise in oxygen fugacity with increasing water content. Since it is well known that higher oxygen fugacities stabilize orthopyroxene (e.g., Berndt et al. 2005; Boudier et al. 2000; Grove and Baker 1984; Grove and Juster 1989) it seems clear that water itself or the change in melt composition destabilizes orthopyroxene in our experiments. The experiments do not allow to distinguish between these effects. However, the melt composition is strongly effected by the water-sensitivity of the stability of plagioclase, which is a key parameter for silica enrichment under water-saturated conditions. Increasing pressure shifts the crystallization temperature of plagioclase to lower temperatures and therefore delays the silica enrichment in the melt and the precipitation of orthopyroxene. This is in accord with the experimental findings of Gaetani et al. (1993, 1994) for a basaltic andesite. Thus, our study supports a model that orthopyroxene-rich rocks can be generated by simple hydration of a tholeiitic basaltic system (e.g. Boudier et al. 2000) only under low pressures, where the oxidizing effect of the hydrations is dominating. Under higher pressures, however, the delay in plagioclase crystallization caused by water resulting in a lower silica activity of the melt becomes more important preventing orthopyroxene crystallization.

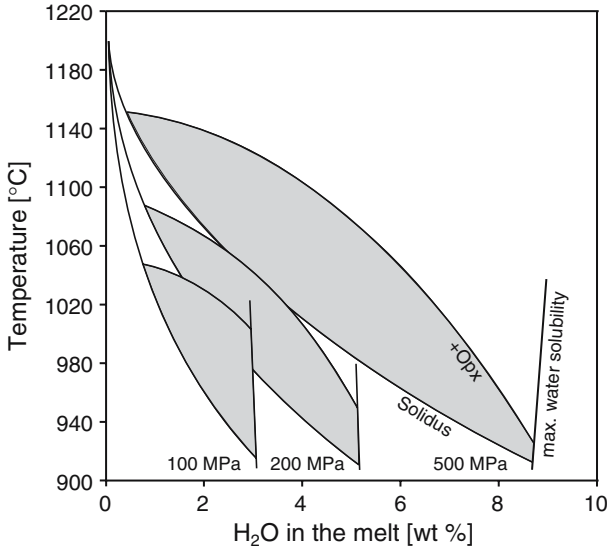

Fig. 12 Stability field of orthopyroxene at different pressures. At low water contents the liquidus temperature is shifted to significantly higher temperatures, whereas water-saturated conditions shift the stability of orthopyroxene to lower temperatures

Effect of H_2O on element partitioning

Ca partitioning between olivine and melt

The amount of calcium in olivine has been the object of many studies (Jurewicz and Watson 1988; Libourel 1999; Longhi et al. 1978; Roeder 1974; Watson 1979). The melt and olivine compositions have the major control on the CaO content, whereas the effects of temperature, pressure and oxygen fugacity are negligible. Libourel (1999) developed a model to calculate the calcium partition coefficient between olivine and melt based on their compositions. The model provides good predictions for dry magmatic systems. In a water-bearing system Berndt et al. (2005) observed a deviation from the predicted values and supposed that water affects the partition coefficient. Our results correlate well with the effects described by Berndt et al. (2005). While the dry experiments, independent of pressure, correspond with the model of Libourel (1999), our water-bearing experiments show a systematic deviation from the calculated values (Fig. 13). This deviation is a function of water in the coexisting melt, which is controlled by the adjusted water activity and by the prevailing pressure. But besides the effect of water, temperature also influences the deviation. At lower temperatures the deviation is smaller.

To separate the effect of temperature from the water effect, we included the forsterite content of olivine into the calcium partitioning calculations. This allows the calcium partitioning to be plotted as a function of temperature (Fig. 14). The effect of water is expressed by a strong increase of calcium partitioning into olivine with decreasing water content. This increase mainly reflects the lower calcium content of olivine in water-bearing systems. In a water diffusion study, Behrens

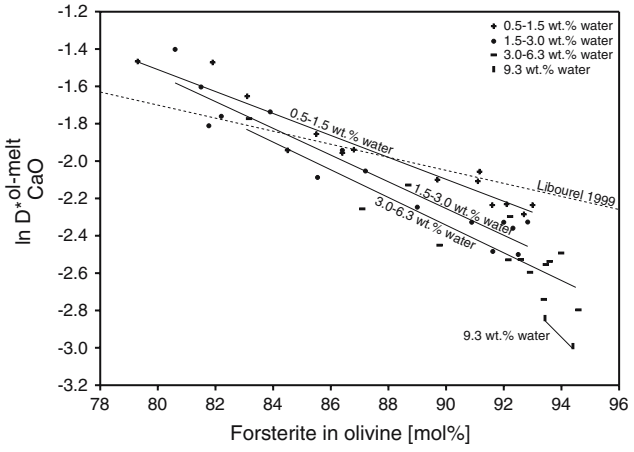

Fig. 13 The influence of the water content of the melt on the Ca-partitioning in olivine. The *dotted line* in the plot belongs to the equilibrium study of (Libourel 1999). The *solid lines* show the water content of the melt of the performed experiments. It is noticeable that their is a significant influence of water on the Ca-partitioning in olivine. With increasing water content, the lnD* ol-melt/CaO value is depressed to lower values

and Schulze (2000) observed a strong bonding of hydrous species on Ca-complexes in the melt. This effect could result in a reduced calcium activity in the melt and thus decreases the calcium content in olivine. However, further experiments at different oxygen fugacities are necessary to determine a systematic effect of the redox-conditions on the calcium partitioning. With the help of an extended database, the calcium partitioning between olivine and melt has the potential to be used as a ''geohygrometer''. A possible application could be the determination of the initial water content of a degassed olivine basalt.

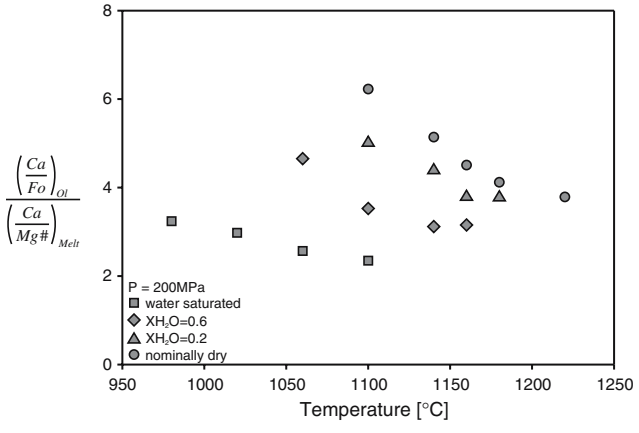

Fig. 14 Molar ratios of Ca/Fo in olivine and Ca/Mg# in the melt are used to illustrate the Ca-partitioning between olivine and melt as a function of temperature. The calculated Ca-partitioning varies systematically with water in the system

Ca/Na partitioning between plagioclase and melt

Sisson and Grove (1993a) showed with melting experiments on a high-alumina basalt that the $K_D^{\text{Plag–Melt}}_{\text{Ca–Na}}$ (calculated using Eq. 2) is very water sensitive, with higher $K_D^{\text{Plag–Melt}}_{\text{Ca–Na}}$ values with increasing amount of water in the melt.

$$K_D^{\text{Plag–Melt}}_{\text{Ca–Na}} = \frac{(\text{Ca/Na})_{\text{plag}}}{(\text{Ca/Na})_{\text{Melt}}} \text{ in mole.} \quad (2)$$

They determined a $K_D^{\text{Plag–Melt}}_{\text{Ca–Na}} = 5.5$ at 200 MPa (~ 6 wt% H_2O in the melt) and a $K_D^{\text{Plag–Melt}}_{\text{Ca–Na}} = 3.4$ at 100 MPa (~ 4 wt% H_2O in the melt). Further experiments under dry conditions and pressures between 800 and 1,200 MPa produced $K_D^{\text{Plag–Melt}}_{\text{Ca–Na}}$ values below 2.0, which infers that the increase in $K_D^{\text{Plag–Melt}}_{\text{Ca–Na}}$ their water-bearing experiments is related to water.

To better understand the effect of bulk composition on the element partitioning, we collected plagioclase-glass pairs from a number of experimental studies showing a wide range in mafic compositions. All were water-saturated (except for 1 atm experiments), and as the pressure mainly controls the water content, an

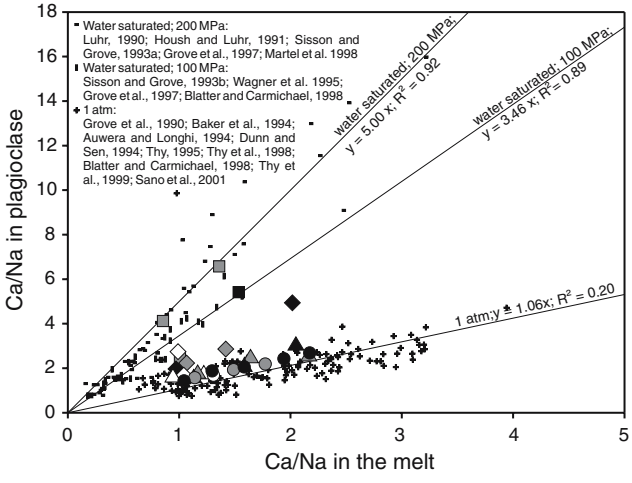

Fig. 15 Effect of water on Ca/Na pairs of plagioclase and the coexisting melt. The different pressures marked in the diagram control the water solubility in the melt. In this diagram, they are used to compare the effect of different water contents on the K_D value. The effect of pressure itself is negligible. The *big symbols* correspond to our experimental study (see Fig. 3 for the signature). The *small symbols* correspond to a number of experimental studies with a huge variety of different compositions (basalts, andesitic basalts, andesites, high alumina basalts, komatites, alkaline basalts). The different compositions deviate only slightly in water solubility and thus plot on the same line. Water shifts the K_D value from ~ 1 (dry conditions) to ~ 3.5 under water-saturated conditions at 100 MPa (~3.2 wt% water) and to ~ 5 under water-saturated conditions at 200 MPa (~5 wt% water), respectively

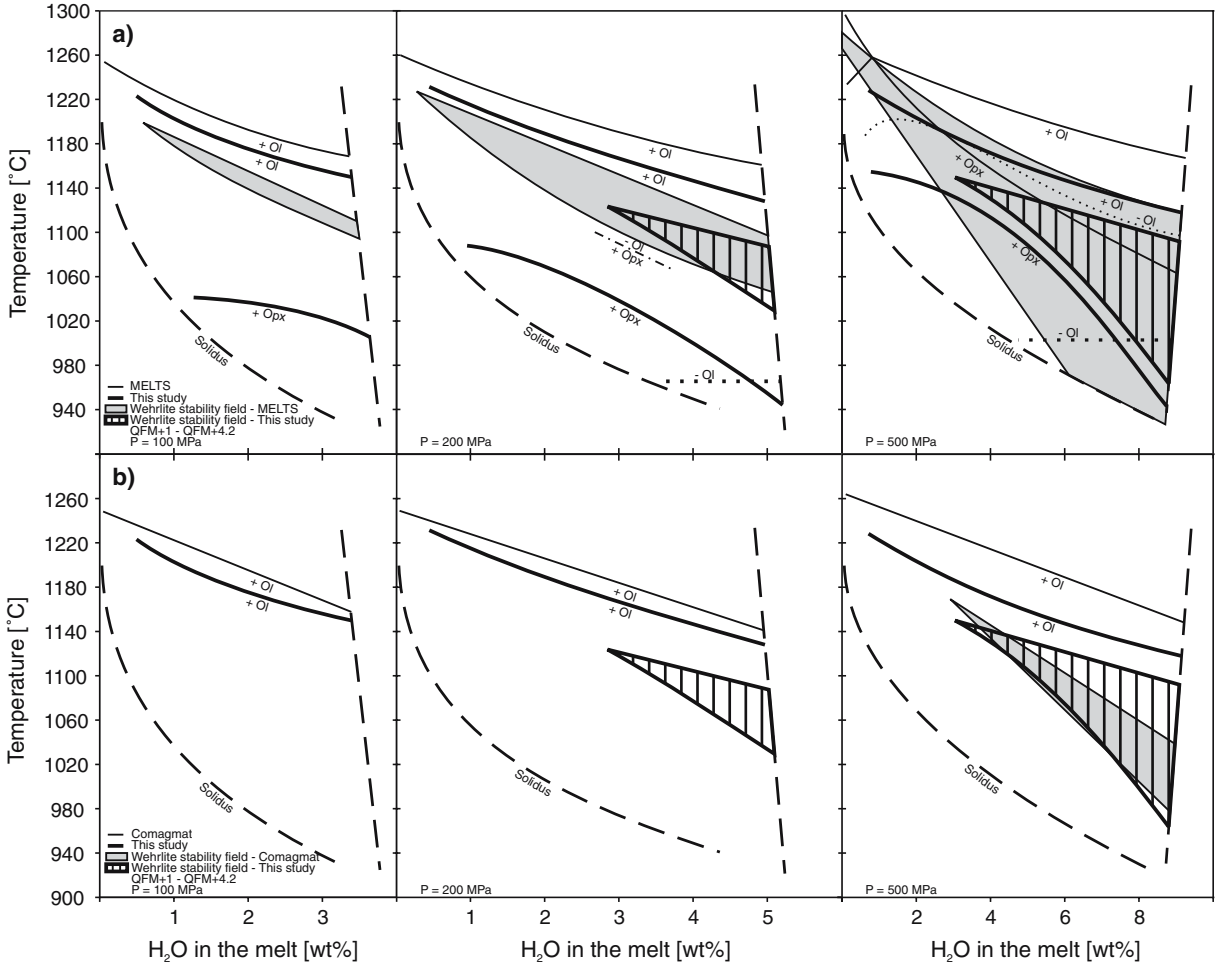

Fig. 16 Phase relations of our system compared with two of the most commonly used models: MELTS (**a**) and Comagmat (**b**). The *thin lines* are calculated phase boundaries, the *thick lines* correspond to our observations. It should be noted that MELTS is only able to predict phase equilibria for redox conditions ≤ QFM + 3. Since those experiments with very high water activity were conducted at higher oxygen fugacities, the corresponding phase equilibria calculated by MELTS was extrapolated

effect of the composition on the water solubility is negligible compared to the scattering of the experiments. At the same pressure (same water content) all compositions have similar $K_{\mathrm{D}}{}^{\mathrm{Plag-Melt}}_{\mathrm{Ca-Na}}$ values (Fig. 15).

In agreement with the study of Berndt et al. (2005), we conclude that the effect of total pressure is negligible. Our ''nominally dry'' experiments should confirm this, as they were prepared with the same procedure and should have the same water content. In these experiments, the determined $K_{\mathrm{D}}{}^{\mathrm{Plag-Melt}}_{\mathrm{Ca-Na}}$ values for the three different pressures are indistinguishable from each other (Fig. 15). To determine the pressure effect it is necessary to perform experiments in a system that is really dry. But as discussed above, iron-bearing systems always contain a certain amount of water.

However, the $K_{\mathrm{D}}{}^{\mathrm{Plag-Melt}}_{\mathrm{Ca-Na}}$ determined from our experiments fit well with the values from others (Fig. 15) indicating that equilibrium was approached in our experiments.

Comparison of the experimental results with thermodynamic models

The experimental results that we provide about the detailed effect of water in the phase proportions and compositions of mafic systems could be incorporated in thermodynamic models. Below we discuss how our results differ from those calculated with currently available thermodynamic calibrations and highlight the problems that one might encounter when applying them to water-rich systems.

Thermodynamic models are often used to calculate phase relations and compositions of magmatic systems. They are used to describe the magmatic evolution including the differentiation paths. Two of the most

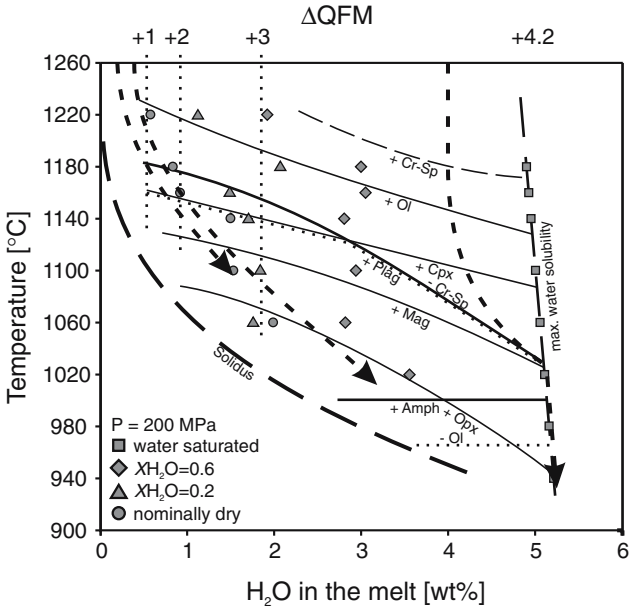

Fig. 17 Determined phase relations at 200 MPa (similar to Fig. 3b), with estimated evolution trends of the system for different water contents of the starting material (0.2, 0.4 and 4 wt%; represented by *arrows*). The shape of the *evolution lines* is estimated from the mass balance calculations of the performed experiments (Table 1)

commonly used models are ''MELTS'' (Ghiorso and Sack 1995) and ''Comagmat'' (Ariskin 1999). ''MELTS'' is a thermodynamic model which performs Gibbs free energy minimization with the use of regular solutions models for both minerals and melt. ''Comagmat'' is a semi-empirical model where the task of equilibrium is solved iteratively for the system of non-linear equilibrium equations and the mass action law using dependencies of equilibrium constants for each mineral–melt reaction on temperature and composition (Ariskin 1999). The lack of a sufficient number of experiments in hydrous mafic systems introduces a large uncertainty in the phase equilibria results of both models (Fig. 16). To compare the calculations of the models with our experimental results, we used the same conditions as in the experiments (fO_2, P, H_2O and equilibrium mode).

''MELTS'' for example slightly overestimates the liquidus temperature for olivine independent of the prevailing water content. In the calculations, the stability of olivine at low temperatures is strongly related to the stability of orthopyroxene. With the strong increase of orthopyroxene stability with pressure the ''olivine-out'' boundary is shifted to much higher temperatures than we have observed.

The phase boundaries of clinopyroxene and plagioclase form the stability field for wehrlites (cumulate rocks consisting of olivine, clinopyroxene ± spinel without plagioclase) shown in Fig. 16. This field is produced by a shift of the stability of plagioclase to lower temperatures due to water. In the experiments, the wehrlitic paragenesis was only observed at pressures > 100 MPa and high water contents. ''MELTS'' overestimates the stability of wehrlites in our system and produces wehrlites even at pressures of 100 MPa and at nearly dry conditions (Fig. 16a).

''Comagmat'' calculates the stability field of olivine well. Even at high water contents, the calculated liquidus depression is in agreement with the experiments. Due to the limitation of the numerical model to ~80% crystal fraction, no orthopyroxene was observed. Compared to the experiments and in contrast to ''MELTS'', ''Comagmat'' underestimates the stability field of wehrlites and produces wehrlites only at pressures > 200 MPa (Fig. 16b).

Evolution trends for different bulk water contents

Since our experiments show that water may significantly influence the phase relations, it is of interest to know how water would affect potential differentiation trends in a primitive tholeiitic basaltic system. Figure 17 shows the estimated evolution trends for a melt with different bulk water contents at a pressure of 200 MPa based on the phase equilibria obtained from our experiments in combination with mass balance calculations. The evolution lines terminate at those conditions where the residual melt fraction is expected to be less than ~ 10 wt%.

At the lowest bulk water content of 0.2 wt%, the estimated evolution trend is practically indistinguishable from the case of completely dry crystallization. Thus, the fractionation/accumulation of crystallized minerals would produce typical troctolitic or gabbroic cumulate rocks as a function of temperature. However, due to the increased water content, both plagioclase and olivine/clinopyroxene would show increased An contents and Mg#, respectively, compared to the dry system.

With a water content of 0.4 wt%, the evolution line is more or less parallel to the above trend, at slightly higher water contents. Fractionation/accumulation of crystallized minerals at temperatures > 1,100°C would produce similar cumulate rocks as before, but with slightly higher An and Mg# in plagioclase and olivine/clinopyroxene, respectively. At temperatures below 1,060°C orthopyroxene crystallizes. At lower temperatures the residual melt has the potential for significant water enrichment reaching the stability field of amphibole at temperatures below ~ 1,000°C. Thus the

probability for forming gabbroic cumulates including interstitial orthopyroxene and/or amphibole is increased.

Starting with a high bulk water content of 4 wt% results in a completely different evolution trend, as illustrated in Fig. 17. The main effect is that the plagioclase-saturation curve is significantly depressed, resulting in a change in the crystallization order and in the co-precipitation of olivine and clinopyroxene without plagioclase. Thus, a potential cumulate rock formed by crystal accumulation at temperatures of ~ 1,100°C would result in typical wehrlite. This aspect is discussed in detail in the next section.

Implications for the origin of wehrlites within the lower oceanic crust

Many ophiolites contain wehrlitic rocks, characteristically intruding the deeper parts of the magmatic section (for details see Nicolas (1989) and references therein). For instance, in the Oman ophiolite, wehrlite bodies were found at different crustal levels from the sheeted dikes down to the Moho transition zone (e.g., Adachi and Miyashita 2001; Juteau et al. 1988). The Mg# of the olivines and clinopyroxene of these rocks are characteristically quite high, often > 90 (Juteau et al. 1988; Koepke et al. 2005a). However, such rocks are rare in drilled or dredged samples of mid-ocean ridges.

In the ophiolite of Macquarie Island, crustal wehrlites are observed as intrusions up to the sheeted dyke level (Jeff Karson, personal communication). This would seem to indicate a water-rich magma in the crustal section, based on our results. The mantle section at Macquarie also shows geochemical characteristics typical of ophiolitic mantle sections, and atypical of mid-oceanic ridge mantle sections (Wertz et al. 2004) and caused by hydrous re-melting and metasomatism of the mantle. Thus, although Macquarie Island appears to be a nearly in-situ slice of mid-ocean ridge, it appears to have had a more hydrous origin than is typical of MORB. This may be related to the highly oblique nature of the plate boundary at that time, though this point is by no means settled.

The origin of wehrlite intrusions within the oceanic crust is not clear. Current models explain the wehrlite bodies as impregnated mantle peridotites (Benn et al. 1988), as cumulates from subduction zone-related tholeiitic basaltic melts (Kelemen et al. 1997), or from picritic melts (Juteau et al. 1988). Studies of Koga et al. (2001) and Koepke et al. (2005a) showed that the clinopyroxenes of the crustal wehrlites from the Oman ophiolite could be in chemical equilibrium with typical MORB and suggest that models involving mantle impregnation or picritic melts are probably not important here.

Since these crustal wehrlites show typical cumulate structures, it is likely that these rocks ''intruded'' as mushes of accumulated crystals in a MORB-type system. To form the critical wehrlite paragenesis of olivine + clinopyroxene ± spinel (without plagioclase) by crystal accumulation in a dry MORB at shallow pressures is nearly impossible, since in ''dry'' MORB melts, plagioclase crystallizes together with olivine, distinctly before the precipitation of clinopyroxene (see previous section). Our experiments show that at pressures > 100 MPa, water changes the crystallization order and forms a field where the wehrlite paragenesis is stable (as shown in Fig. 3). The corresponding olivines and clinopyroxenes typically show high Mg# (up to ~ 93 mole% Fo in olivine). This agrees with the phase compositions of natural wehrlites from the Oman ophiolite (Koepke et al. 2005a; Koga et al. 2001). Thus, the experiments suggest that typical crustal wehrlites present in many ophiolites could be interpreted as cumulates of very water-rich tholeiitic melts, formed at pressures > 100 MPa, temperature ~ 1,060°C and water contents of more than 3 wt%.

For this model, special requirements are necessary, since it is well known that typical MORB is more or less dry with water contents significantly below the 3 wt% mentioned above. There are two possible origins for the water-enrichment in MORB melts under the ridges. First, high water contents can be achieved in MORB melts generated above subduction zones, which in principle can be related to spreading systems from fore-arc or marginal basin settings (e.g., Ishikawa et al. 2002; Lachize et al. 1996; Miyashiro 1974; Nicolas 1989; Pearce et al. 1984). Second, there is more and more evidence supporting a model that aqueous fluids derived from seawater may penetrate into magma chambers beneath ridges (Benoit et al. 1999; Bosch et al. 2004; Boudier et al. 2005; Koepke et al. 2005c; Koepke et al. 2005b; Koga et al. 2001; Nicolas and Mainprice 2005; Nicolas et al. 2003; Nonnotte et al. 2005). For these reasons, further investigation of water-bearing MORB systems, particularly at lower fO_2, is likely to prove fruitful for understanding the magmatic evolution of mid-ocean ridges.

Conclusions

Water dramatically influences the phase equilibria of a tholeiitic basaltic system, and therefore magmatic processes at mid-ocean ridges and marginal basins in general. The results of this study support many of the

well-known effects with water, like depression of liquidus and solidus, increasing melt fraction at a given temperature, depressing the saturation of plagioclase, changing of the liquid lines of descent, and influencing the element partitioning between crystals and melt.

This study defines clearly the shifting of phase boundaries and mineral compositions as a systematic function of water content between ''dry'' conditions and water saturation. These conditions correspond somewhat indirectly to the conditions of actual MORB formation, as the oxygen fugacity studied here was higher than those thought to be characteristic of MORB. However, these results delineate the general trends of petrogenesis in hydrous basaltic systems.

One interesting result of our investigation is a re-investigation of the term ''dry''. We realized that the melt compositions of even nominally dry runs still contained up to half a percent of water. In many previous experiments conducted under ''dry'' conditions, the content of water was never actually measured, but simply assumed to be zero. For example, nominally anhydrous high pressure experiments performed in Piston Cylinder apparatus are often not absolutely water-free (Hirschmann et al. 1998; Holtz et al. 2001; Kagi et al. 2005). This may result in a considerable amount of water-induced fluctuation in the current experimental literature that should be investigated more fully.

The genesis of wehrlites in the ocean crust is more than just academic in nature. Wehrlites are a component of most ophiolites, but are extremely rare to nonexistent in samples dredged and drilled from modern ocean crust *in situ*. This has led many researchers to assert that wehrlites are present even in dry mid-ocean ridge systems, but are simply not dredgeable or drillable because of their location in the mid-segment lower crust. Our results suggest that this difference between ophiolites and ocean crust is a critical one, since a high water content is truly required for the generation of wehrlites. This is not to suggest that wehrlite formation at mid-ocean ridges is impossible, but it seems unlikely that large volumes of it are hiding somewhere beneath most mid-ocean ridges. Macquarie Island seems to be an exception to this (Wertz et al. 2004).

Another result of this work is the effect of water on Ca partitioning into olivine. In principle, with further work, it should be possible to calibrate a ''geohygrometer'' based on this effect that should be of great use in determining the water content of subaerial basalts and those oceanic basalts which reach water saturation during eruption and degas. A surprising number of MORB samples, even form relatively deep water show large scale vesicle formation. If the water content of erupted basalts could be measured post hoc, then the vesicularity and residual water content of ocean floor basalts might well be useful in determining the eruption history.

The results from this study show significant departures of the temperatures of crystallization and the compositions of phases crystallized to those predicted by hybrid thermodynamic/empirical and purely empirical models such as ''MELTS'' and ''Comagmat''. This is to be expected, since the lack of observations in this region of pressure-temerature-composition space were one of the motivating factors of this study. One benefit of this study is that these data represent an internally consistent data set for a primitive tholeiitic basaltic system in terms of temperature, water content, and pressure. Thus, these data should serve to improve future models. The next critical step in the exploration of tholeiitic systems will be a parallel set of water-bearing experiments in the same system at lower fO_2 under otherwise similar conditions. This study covering a redox range from QFM-3 to QFM+2 is in progress.

Acknowledgments Otto Diedrich's careful sample preparation is gratefully acknowledged. The authors thank F. Costa Rodriguez and B. Scaillet for careful and thorough reviews of the manuscript. Valuable editorial advice from J. Hoefs is acknowledged. This research used sample was provided by the Ocean Drilling Program (ODP). ODP is sponsored by the US National Science Foundation (NSF) and participating countries under management of Joint Oceanographic Institutions (JOI), Inc. The funding for this research was provided by a grant from the Deutsche Forschungsgemeinschaft (KO 1723/4-2). Jonathan E. Snow was supported by a Heisenberg Fellowship from the Deutsche Forschungsgemeinschaft.

References

Adachi Y, Miyashita S (2001) Magmatic processes of layered gabbro in the northern Oman ophiolite inferred from the zoning of plagioclase. International conference geology of Oman Abstract, vol 6

Albarède F, Provost A (1977) Petrological and geochemical mass-balance equations: an algorithm for least-square fitting and general error analysis. Comput Geosci 3:309–326

Ariskin AA (1999) Phase equilibria modeling in igneous petrology: use of COMAGMAT model for simulating fractionation of ferro-basaltic magmas and the genesis of high-alumina basalt. J Volcanol Geotherm Res 90:115–162

Asimow PD, Langmuir CH (2003) The importance of water to oceanic mantle melting regimes. Nature 421:815–820

Auwera JV, Longhi J (1994) Experimental study of a jotunite (hypersthene monzodiorite): constraints on the parent magma composition and crystallization conditions (P, T, fO2) of the Bjerkreim–Sokndal layered intrusion (Norway). Contrib Mineral Petrol 118:60–78

Baker MB, Grove TL, Price R (1994) Primitive basalts and andesites from the Mt. Shasta region, N California: products of varying melt fraction and water content. Contrib Mineral Petrol 118:111–129

Behrens H, Schulze F (2000) Compositional dependence of water diffusivity in aluminosilicate glasses and melts. In: D. Rammlmair JM, Oberthür Th, Heimann RB, Pentinghaus H (eds) Applied mineralogy in research, economy, technology and culture, Proceedings of the 6th international conference on applied mineralogy, Balkema, Rotterdam, pp 95–98

Bell DR, Rossman GR (1992) Water in earth's mantle: the role of nominally anhydrous minerals. Science 255:1391–1397

Benn K, Nicolas A, Reuber I (1988) Mantle crust transition zone and origin of wehrlitic magmas: evidence from the Oman ophiolite. Tectonophysics 151:75–85

Benoit M, Ceuleneer G, Polve M (1999) The remelting of hydrothermally altered peridotite at mid-ocean ridges by intruding mantle diapirs. Nature 402:514–518

Berndt J, Liebske C, Holtz F, Freise M, Nowak M, Ziegenbein D, Hurkuck W, Koepke J (2002) A combined rapid-quench and H_2-membrane setup for internally heated pressure vessels: Description and application for water solubility in basaltic melts. Am Mineral 87:1717–1726

Berndt J, Koepke J, Holtz F (2005) An experimental investigation of the influence of water and oxygen fugacity on differentiation of MORB at 200 MPa. J Petrol 46:135–167

Bezos A, Humler E (2005) The Fe^{3+}/σ Fe ratios of MORB glasses and their implications for mantle melting. Geochim Cosmochim Acta 69:711–725

Blatter DL, Carmichael ISE (1998) Plagioclase-free andesites from Ziticuaro (Michoacan), Mexico: petrology and experimental constraints. Contrib Mineral Petrol 132:121–138

Blundy JD, Holland TJB (1990) Calcic amphibole equilibria and a new amphibole-plagioclase geothermomemeter. Contrib Mineral Petrol 104:208–224

Bosch D, Jamais M, Boudier F, Nicolas A, Dautria JM, Agrinier P (2004) Deep and high-temperature hydrothermal circulation in the Oman ophiolite: petrological and isotopic evidence. J Petrol 45:1181–1208

Boudier F, Godard M, Armbruster C (2000) Significance of gabbronorite occurrence in the crustal section of the Semail ophiolite. Mar Geophys Res 21:307–326

Boudier FO, Nicolas A, Mainprice D (2005) Does anisotropy of thermal contraction control hydrothermal circulation at the moho level below fast spreading oceanic ridges? Int Geol Rev 47:101–112

Burnham WC (1979) The importance of volatile constituents. In: Yoder HS (ed) The evolution of the igneous rocks: fiftieth anniversary perspectives. Princeton University Press, Princeton, pp 439–482

Chou IM (1987) Oxygen buffer and hydrogen sensor techniques at elevated pressures and temperatures. In: Ulmer GC, Barnes HL (eds) Hydrothermal experimental techniques. Wiley, New York, pp 61–99

Christie DM, Carmichael ISE, Langmuir CH (1986) Oxidation states of mid-ocean ridge basalt glasses. Earth Planet Sci Lett 79:397–411

Coogan LA, Wilson RN, Gillis KM, MacLeod CJ (2001) Near-solidus evolution of oceanic gabbros: Insights from amphibole geochemistry. Geochim Cosmochim Acta 65:4339–4357

Danyushevsky LV (2001) The effect of small amounts of H_2O crystallisation of mid-ocean ridge and backarc basin magmas. J Volcanol Geotherm Res 110:265–280

Danyushevsky LV, Eggins SM, Falloon TJ, Christie DM (2000) H_2O abundance in depleted to moderately enriched mid-ocean ridge magmas; Part I: Incompatible behaviour, implications for mantle storage, and origin of regional variations. J Petrol 41:1329–1364

Devine JD, Gardner JE, Brack HP, Layne GD, Rutherford MJ (1995) Comparison of microanalytical methods for estimating H_2O contents of silicic volcanic glasses. Am Mineral 80:319–328

Dick HJB, Natland JH, Alt JC, Bach W, Bideau D, Gee JS, Haggas S, Hertogen JGH, Hirth G, Holm PM, Ildefonse B, Iturrino GJ, John BE, Kelley DS, Kikawa E, Kingdon A, LeRoux PJ, Maeda J, Meyer PS, Miller DJ, Naslund HR, Niu Y, Robinson PT, Snow J, Stephen RA, Trimby PW, Worm H-U, Yoshinobu A (2000) A long in situ section of the lower ocean crust: results of ODP Leg 176 drilling at the Southwest Indian Ridge. Earth Planet Sci Lett 179:31–51

Dunn T, Sen C (1994) Mineral/matrix partition-coefficients for orthopyroxene, plagioclase, and olivine in basaltic to andesitic systems: a combined analytical and experimental study. Geochim Cosmochim Acta 58:717–733

Eggler DH, Burnham CW (1973) Crystallization and fractionation trends in system andesite-H_2O – CO_2 – O_2 at pressures to 10 Kb. Geol Soc Am Bull 84:2517–2532

Ernst WG, Liu J (1998) Experimental phase-equilibrium study of Al- and Ti-contents of calcic amphibole in MORB: a semi-quantitative thermobarometer. Am Mineral 83:952–969

Gaetani GA, Grove TL, Bryan WB (1993) The influence of water on the petrogenesis of subduction-related igneous rocks. Nature 365:332–334

Gaetani GA, Grove TL, Bryan WB (1994) Experimental phase relations of basaltic andesite from Hole 839B under hydrous and anhydrous conditions. In: Hawkins J, Parson L, Allan J, et al. (eds) Proceedings of the Ocean Drilling Program, scientific results, vol 135. Ocean Drilling Program, College Station, TX, pp 557–563

Ghiorso MS, Sack RO (1995) Chemical mass transfer in magmatic processes IV. A revised and internally consistent thermodynamic model for the interpolation and extrapolation of liquid–solid equilibria in magmatic systems at elevated temperatures and pressures. Contrib Mineral Petrol 119:197–212

Grove TL, Baker MB (1984) Phase-equilibrium controls on the tholeiitic versus calc-alkaline differentiation trends. J Geophys Res 89:3253–3274

Grove TL, Bryan WB (1983) Fractionation of pyroxene-phyric MORB at low pressure: an experimental study. Contrib Mineral Petrol 84:293–309

Grove TL, Juster TC (1989) Experimental investigations of low-Ca pyroxene stability and olivine pyroxene liquid equilibria at 1-atm in natural basaltic and andesitic liquids. Contrib Mineral Petrol 103:287–305

Grove TL, Kinzler RJ, Bryan WB (1990) Natural and experimental phase relations of lavas from Serocki Volcano. In: Bryan WB, Juteau T et al. (eds) Proceeding of the Ocean Drilling Program, vol 106/109 Part B. Ocean Drilling Program, College Station, TX, pp 9–17

Grove TL, Donnelly-Nolan JM, Housh T (1997) Magmatic processes that generated the rhyolite of Glass Mountain, Medicine Lake volcano, N California. Contrib Mineral Petrol 127:205–223

Hamilton DL, Burnham CW, Osborn EF (1964) The solubility of water and effects of oxygen fugacity and water content on crystallization in mafic magmas. J Petrol 5:21–39

Helz RT (1973) Phase relations of basalt in their melting ranges at P_H2O = 5 kb as a function of oxygen fugacity. J Petrol 14:249–302

Helz RT (1976) Phase relations of basalt in their melting ranges at P_{H2O} = 5 kb. Part II: melt compositions. J Petrol 17:139–193

Hirschmann MM, Baker MB, Stolper E (1998) The effect of alkalis on the silica content of mantle-derived melts. Geochim Cosmochim Acta 62:883–902

Hirschmann MM, Aubaud C, Withers AC (2005) Storage capacity of H_2O in nominally anhydrous minerals in the upper mantle. Earth Planet Sci Lett 236:167–181

Holloway JR, Burnham CW (1972) Melting relations of basalt with equilibrium water pressure less than total pressure. J Petrol 13:1–29

Holloway JR, Dixon JE, Pawley AR (1992) An internally heated, rapid-quench, high-pressure vessel. Am Mineral 77:643–646

Holtz F, Behrens H, Dingwell DB, Johannes W (1995) H_2O solubility in haplogranitic melts - compositional, pressure, and temperature dependence. Am Mineral 80:94–108

Holtz F, Becker A, Freise M, Johannes W (2001) The water-undersaturated and dry Qz-Ab-Or system revisited. Experimental results at very low water activities and geological implications. Contrib Mineral Petrol 141:347–357

Housh TB, Luhr JF (1991) Plagioclase-melt equilibria in hydrous systems. Am Mineral 76:477–492

Huebner JS, Sato M (1970) Oxygen fugacity-temperature relationships of manganese oxide and nickel oxide buffers. Am Mineral 55:934–952

Ishikawa T, Nagaishi K, Umino S (2002) Boninitic volcanism in the Oman ophiolite: Implications for thermal condition during transition from spreading ridge to arc. Geology 30:899–902

Jurewicz AJG, Watson EB (1988) Cations in olivine: 1. Calcium partitioning and calcium-magnesium distribution between olivines and coexisting melts, with Petrologic Applications. Contrib Mineral Petrol 99:176–185

Juster TC, Grove TL, Perfit MR (1989) Experimental constraints on the generation of Fe–Ti basalts, andesites, and rhyodacites at the Galapagos spreading centre, 85°W and 95°W. J Geophys Res 94:9251–9274

Juteau T, Ernewein M, Reuber I, Whitechurch H, Dahl R (1988) Duality of magmatism in the plutonic sequence of the Sumail Nappe, Oman. Tectonophysics 151:107–135

Kagi R, Müntener O, Ulmer P, Ottolini L (2005) Piston-cylinder experiments on H_2O undersaturated Fe-bearing systems: an experimental setup approaching fO_2 conditions of natural calc-alkaline magmas. Am Mineral 90:708–717

Kawamoto T (1996) Experimental constraints on differentiation and H_2O abundance of calc-alkaline magmas. Earth Planet Sci Lett 144:577–589

Kawamoto T, Hirose K (1994) Au-Pd sample containers for melting experiments on iron and water-bearing systems. Eur J Mineral 6:381–385

Kelemen PB, Koga K, Shimizu N (1997) Geochemistry of gabbro sills in the crust-mantle transition zone of the Oman ophiolite: implications for the origin of the oceanic lower crust. Earth Planet Sci Lett 146:475–488

Koepke J, Feig ST, Snow J, Freise M (2004) Petrogenesis of oceanic plagiogranites by partial melting of gabbros: an experimental study. Contrib Mineral Petrol 146:414–432

Koepke J, Feig ST, Boudier F, Hellebrand E (2005a) Experimental study on crustal wehrlites of the Oman ophiolite: experimental outline and microanalytical results. Ofioliti 30:197–198

Koepke J, Feig ST, Snow J (2005b) Hydrous partial melting within the lower oceanic crust. Terra Nova 17:286–291

Koepke J, Feig ST, Snow JE (2005c) Late stage magmatic evolution of oceanic gabbros as a result of hydrous partial melting: evidence from the Ocean Drilling Program (ODP) Leg 153 drilling at the Mid-Atlantic Ridge. Geochem Geophys Geosyst 6:2004 GC000805

Koga KT, Kelemen PB, Shimizu N (2001) Petrogenesis of the crust-mantle transition zone and the origin of lower crustal wehrlite in the Oman ophiolite. Geochem Geophys Geosyst 2:2000 GC000132

Kovalenko VI, Naumov VB, Yarmolyuk VV, Dorofeeva VA (2000) Volatile components (H_2O, CO_2, Cl, F, and S) in basic magmas of various geodynamic settings: Data on melt inclusions and quenched glasses. Petrology 8:113–144

Kress VC, Carmichael ISE (1991) The compressibility of silicate liquids containing Fe_2O_3 and the effect of composition, temperature, oxygen fugacity and pressure on their redox states. Contrib Mineral Petrol 108:82–92

Lachize M, Lorand JP, Juteau T (1996) Calc-alkaline differentiation trend in the plutonic sequence of the Wadi Haymiliyah section, Haylayn massif, Semail ophiolite, Oman. Lithos 38:207–232

Leake BE, Woolley AR, Arps CES, Birch WD, Gilbert MC, Grice JD, Hawthorne FC, Kato A, Kisch HJ, Krivovichev VG, Linthout K, Laird J, Mandarino JA, Maresch WV, Nickel EH, Rock NMS, Schumacher JC, Smith DC, Stephenson NCN, Ungaretti L, Whittaker EJW, Guo YZ (1997) Nomenclature of amphiboles: report of the subcommittee on amphiboles of the International Mineralogical Association, commission on new minerals and mineral names. Am Mineral 82:1019–1037

Leschik M, Heide G, Frischat GH, Behrens H, Wiedenbeck M, Wagner N, Heide K, Geissler H, Reinholz U (2004) Determination of H_2O and D_2O contents in rhyolitic glasses. Phys Chem Glass 45:238–251

Libourel G (1999) Systematics of calcium partitioning between olivine and silicate melt: implications for melt structure and calcium content of magmatic olivines. Contrib Mineral Petrol 136:63–80

Lindsley DH (1983) Pyroxene Thermometry. Am Mineral 68:477–493

Longhi J, Walker D, Hays JF (1978) Distribution of Fe and Mg between olivine and lunar basaltic liquids. Geochim Cosmochim Acta 42:1545–1558

Luhr JF (1990) Experimental phase-relations of water-saturated and sulfur-saturated arc magmas and the 1982 eruptions of El-Chichon volcano. J Petrol 31:1071–1114

Mandeville CW, Webster JD, Rutherford MJ, Taylor BE, Timbal A, Faure K (2002) Determination of molar absorptivities for infrared absorption bands of H_2O in andesitic glasses. Am Mineral 87:813–821

Martel C, Pichavant M, Bourdier JL, Traineau H, Holtz F, Scaillet B (1998) Magma storage conditions and control of eruption regime in silicic volcanoes: experimental evidence from Mt. Pelee. Earth Planet Sci Lett 156:89–99

Miyashiro A (1974) Volcanic rock series in island arcs and active continental margins. Am J Sci 274:321–355

Natland JH, Dick HJB (2002) Stratigraphy and composition of gabbros drilled in Ocean Drilling Program Hole 735B, Southwest Indian Ridge: a synthesis of geochemical data. In: Natland JH, Dick HJB, Miller DJ, Von Herzen RP (eds) Proceedings of the ODP, scientific results, vol 176, pp 1–69 (online). http://www.odp.tamu.edu/publications/176_SR/VOLUME/ SYNTH/SYNTH.PDF

Natland JH, Meyer PS, Dick HJB, Bloomer SH (1991) Magmatic oxides and sulfides in gabbroic rocks from Hole 735B and the later development of the liquid line of descent. In: Von Herzen RP, Robinson PT et al. (eds) Proceedings of the ODP, scientific results, vol 118, Ocean Drilling Program, College Station, TX, pp 75–111

Nicolas A (1989) Structures of ophiolites and dynamics of oceanic lithosphere. In: Kluver Academic, Dordrecht, p 367

Nicolas A, Mainprice D (2005) Burst of high-temperature seawater injection throughout accreting oceanic crust: a case study in Oman ophiolite. Terra Nova 17:326–330

Nicolas A, Mainprice D, Boudier F (2003) High-temperature seawater circulation throughout crust of oceanic ridges: a model derived from the Oman ophiolites. J Geophys Res Solid Earth 108:2371

Nonnotte P, Ceuleneer G, Benoit M (2005) Genesis of andesitic-boninitic magmas at mid-ocean ridges by melting of hydrated peridotites: geochemical evidence from DSDP Site 334 gabbronorites. Earth Planet Sci Lett 236:632–653

Ohlhorst S, Behrens H, Holtz F (2001) Compositional dependence of molar absorptivities of near-infrared OH- and H_2O bands in rhyolitic to basaltic glasses. Chem Geol 174:5–20

Panjasawatwong Y, Danyushevsky LV, Crawford AJ, Harris KL (1995) An experimental study of the effects of melt composition on plagioclase–melt equilibria at 5 kbar and 10 kbar: implications for the origin of magmatic high-An plagioclase. Contrib Mineral Petrol 118:420–432

Pearce JA, Lippard SJ, Roberts S (1984) Characteristics and tectonic significance of supra-subduction zone ophiolites. In: Kokelaar BP, Howells MJ (eds) Marginal basin geology. Blackwell, London, pp 77–94

Pitzer KS, Sterner SM (1994) Equations of state valid continuously from zero to extreme pressures for H_2O and CO_2. J Chem Phys 101:3111–3116

Pouchou JL, Pichoir F (1991) Quantitative analysis of homogeneous or stratified microvolumes applying the model ''PAP''. In: Heinrich KFJ, Newbury DE (eds) Electron probe quantification. Plenum Press, New York, pp 31–75

Putirka K, Johnson M, Kinzler R, Longhi J, Walker D (1996) Thermobarometry of mafic igneous rocks based on clinopyroxene–liquid equilibria, 0–30 kbar. Contrib Mineral Petrol 123:92–108

Putirka KD, Mikaelian H, Ryerson F, Shaw H (2003) New clinopyroxene–liquid thermobarometers for maric, evolved, and volatile-bearing lava compositions, with applications to lavas from Tibet and the Snake River Plain, Idaho. Am Mineral 88:1542–1554

Robie RA, Hemingway BS, Fisher JR (1978) Thermodynamic properties of minerals and related substances at 298,15 K and 1 Bar (10^5 Pascals) pressure and at higher temperatures. Geol Surv Bull 1452, 456 pp

Roeder PL (1974) Activity of iron and olivine solubility in basaltic liquids. Earth Planet Sci Lett 23:397–410

Roeder PL, Emslie RF (1970) Olivine–liquid equilibrium. Contrib Mineral Petrol 29:275–289

Rollinson H, Appel PWU, Frei R (2002) A metamorphosed, early Archaean chromitite from west Greenland: implications for the genesis of Archaean anorthositic chromitites. J Petrol 43:2143–2170

Roux J, Lefevre A (1992) A fast-quench device for internally heated pressure vessels. Eur J Mineral 4:279–281

Saal AE, Hauri EH, Langmuir CH, Perfit MR (2002) Vapour undersaturation in primitive mid-ocean-ridge basalt and the volatile content of Earth's upper mantle. Nature 419:451–455

Sano T, Fujii T, Deshmukh SS, Fukuoka T, Aramaki S (2001) Differentiation processes of Deccan Trap basalts: contribution from geochemistry and experimental petrology. J Petrol 42:2175–2195

Scaillet B, Pichavant M, Roux J (1995) Experimental crystallization of leukogranite magmas. J Petrol 36:663–705

Scholze H (1959) Über die quantitative ir-spektroskopische Wasserbestimmung in Silicaten. Angew Chem Int Edit 71:678–678

Schwab RG, Küstner D (1981) The equilibrium fugacities of important oxygen buffers in technology and petrology. N Jb Miner Mh 140:112–142

Shaw HR, Wones DR (1964) Fugacity coefficients for hydrogen gas between 0°C and 1000°C, for pressures to 3000 atm. Am J Sci 262:918–929

Shipboard Scientific Party (2004) Drilling mantle peridotites along the mid-atlantic ridge from 14° to 16°N. In: Kelemen PB, Kikawa E, Miller DJ et al. (eds) Proceedings of the Ocean Drilling Program, initial reports, vol 209. Ocean Drilling Program, College Station, TX, pp 1–139

Sisson TW, Grove TL (1993b) Temperatures and H_2O contents of low-MgO high-alumina basalts. Contrib Mineral Petrol 113:167–184

Sisson TW, Grove TL (1993a) Experimental investigations of the role of H_2O in calc-alkaline differentiation and subduction zone magmatism. Contrib Mineral Petrol 113:143–166

Snow JE (2002) Major and trace element evolution of Hole 735B gabbros. In: Natland JH, Dick HJB, Miller DJ, Von Herzen RP (eds) Proceedings of the Ocean Drilling Program, scientific results, vol 176, pp 1–18 (online). http://www.odp.tamu.edu/ publications/176_SR/VOLUME/CHAPTERS/SR176_12.PDF

Snyder D, Carmichael ISE, Wiebe RA (1993) Experimental study of liquid evolution in an Fe-rich, layered mafic intrusion: constraints of Fe-Ti oxide precipitation on the T – fO_2 and T-ρpaths of tholeiitic magmas. Contrib Mineral Petrol 113:73–86

Sobolev AV, Chaussidon M (1996) H_2O concentration in primary melts from supra-subduction zones and mid-ocean ridges: Implication for H_2O storage and recycling in the mantle. Earth Planet Sci Lett 137:45–55

Spulber SD, Rutherford MJ (1983) The origin of rhyolite and plagiogranite in oceanic crust: an experimental study. J Petrol 24:1–25

Stormer JC (1983) The effects of recalculation on estimates of temperature and oxygen fugacity from analyses of multicomponent iron titanium-oxides. Am Mineral 68:586–594

Thy P (1995) Low-pressure experimental constraints on the evolution of komatiites. J Petrol 36:1529–1548

Thy P, Lesher CE, Fram MS (1998) Low pressure experimental constraints on the evolution of basaltic lavas from Site 917, southeast Greenland continental margin. In: Saunders AD, Larsen HC, Wise SW Jr (eds) Proceedings of the ODP, scientific results, vol 152. Ocean Drilling Program, College Station, TX, pp 359–372

Thy P, Lesher CE, Mayfield JD (1999) Low-pressure melting studies of basalt and basaltic andesite from the southeast Greenland continental margin and the origin of dacites at site 917. In: Larsen HC, Duncan RA, Allan JF, Brooks K (eds) Proceedings of the ODP, scientific results, vol 163. Ocean Drilling Program, College Station, TX, pp 95–112

Toplis MJ (2005) The thermodynamics of iron and magnesium partitioning between olivine and liquid: criteria for assessing and predicting equilibrium in natural and experimental systems. Contrib Mineral Petrol 149:22–39

Toplis MJ, Carroll MR (1995) An experimental study of the influence of oxygen fugacity on Fe-Ti oxide stability, phase relations, and mineral-melt equilibra in ferro-basaltic systems. J Petrol 36:1137–1170

Tribuzio R, Tiepelo M, Thirlwall MF (2000) Origin of titanian pargasite in gabbroic rocks from the Northern Apennine ophiolites (Italy): Insight into the late-magmatic evolution of a MOR-type intrusive sequence. Earth Planet Sci Lett 176:281–293

Wagner TP, Donnellynolan JM, Grove TL (1995) Evidence of hydrous differentiation and crystal accumulation in the low-MgO, high-Al_2O_3 Lake basalt from Medicine Lake volcano, California. Contrib Mineral Petrol 121:201–216

Watson EB (1979) Calcium diffusion in a simple silicate melt to 30 Kbar. Geochim Cosmochim Acta 43:313–322

Wertz K, Hellebrand E, Snow JE, von der Handt A, Mosher S (2004) Implications of spoon-shaped rare earth pattern in Macquarie Island depleted residual peridotites. Geological Society of Australia Ann. Mtg 2004, Hobart, Tasmania